Resonance in a Finite Volume in Quantum Chromodynamics

Anthony C. -P. Hsu

Supervisors:

Anthony W. Thomas

Ross D. Young

Department of Physics

The University of Adelaide

Abstract

Quantum chromodynamics (QCD) is a theory which describes the strong interactions of the quarks. When the energy is lower than about 1 GeV, the QCD coupling become so large that we can not study it perturbatively. Lattice QCD can be used to study QCD non-perturbatively and is suitable for the low energy region.

Much remains to be studied in QCD, such as resonances in scattering processes. Lüscher's formula can relate the scattering process in finite volume lattices with phase shifts in the infinite volume scattering in the real world. In this study, we will construct a model for $\pi - \pi$ scattering on a lattice. We will use this model to investigate Lüscher's approach. $\rho \to \pi\pi$, and $\rho \to \pi\omega$ channels in the $J = 1$ isovector $\pi - \pi$ scattering will be considered.

Statement of Originality

This work contains no material which has been accepted for the award of any other degree or diploma in any university or other tertiary institution and, to the best of my knowledge and belief, contains no material previously published or written by another person, except where due reference has been made in the text.

I give consent to this copy of my thesis when deposited in the University Library, being made available for loan and photocopying, subject to the provisions of the Copyright Act 1968.

The author acknowledges that copyright of published works contained within this thesis resides with the copyright holder(s) of those works.

I also give permission for the digital version of my thesis to be made available on the web, via the University's digital research repository, the Library catalogue and also through web search engines, unless permission has been granted by the University to restrict access for a period of time.

Anthony Chi-Pin Hsu

Acknowledgements

I would firstly like to thank my supervisors Anthony Thomas and Ross Young for their invaluable directions. I would like to thank Jonathan Hall for his constant help and for his reading of the thesis. I would also like to thank my mother You-Yu Hsiung for her total support.

Contents

Chapter 1

Introduction

1.1 Prelude

There are four basic forces in the universe, namely electromagnetism, the weak interaction, the strong interaction, and gravity. The Standard Model (SM) developed in the twentieth century unifies the first three of them, electromagnetism, the weak interaction, and the strong interaction. Although theories have been developed to include the remaining force, the inclusion of gravity still needs further investigations.

The known world of matter is composed of quarks and leptons. In the Standard Model, leptons, such as electrons, undergo the influence of electromagnetism and the weak interaction, while quarks experience one more force, the strong interaction. Quarks are bound together by the strong interaction, forming hadrons. Hadrons, in turn, can be categorized into baryons, composed of three quarks, and mesons, composed of a quark and an antiquark.

The two most common hadrons are the protons and neutrons. They are the components of the atomic nuclei. Protons and neutrons are composed of up quarks and down quarks. Besides protons and neutrons, there are other hadrons with higher energies, which are referred to as resonances.

The sign of the existence of the resonances can be found in scattering experiments. For example, an experiment in the Brookhaven National Laboratory in which a K^- meson interacted with a proton led to the discovery of the resonance Ω^-.[1][2] Since the existence of the resonances are largely due to the strong interaction, which binds their components together, these resonances can provide us with good information for studying the strong interaction. However, there is still much to learn about them.[3]

Fig. 1.1.1 The discovery of Ω^- in the bubble chamber photo on the left and a diagram of particle tracks on the right. Photo courtesy Brookhaven National Laboratory.[4]

We can study the resonances with quantum chromodynamics (QCD), a theory describing the strong interaction, which plays an important role in these hadrons. QCD can be studied perturbatively when the coupling constant in the strong interaction is not large. However, this is not the case for energy region below about 1 GeV.[5] The masses of many resonances are situated in this energy region. While QCD can not be studied perturbatively in this region, we can investigate it with the help of lattice QCD.

A scattering process can be modelled in a finite volume lattice with imposed boundary conditions. Such lattices have states with a discretized energy spectrum from which phase shifts can be extracted. Martin Lüscher proposed a method to calculate the phase shifts assuming that the finite volume effect is small. Thus, Lüscher's formula relates the phase shift of infinite volume scattering in the real world with the finite volume model. We would like to compare the finite volume resonant phase shifts acquired by Lüscher's formula with the phase shifts of the infinite volume case.

1.2 Overview of Contents

We will start with a simple model involving the scattering of two pions in the presence of a fictious low-lying sigma resonance. The mass of the pion is about

0.138 GeV,[6] well within the lower energy region for QCD where perturbative methods can not be applied. The scattering process will be studied on a lattice with periodic boundary conditions imposed on it.

In Chapter 2, we first introduce the setting of the lattice. We are going to see the effects of imposing a lattice with periodic boundary conditions on a scattering process. We will review the theoretical background of Lüscher's formula. The employment of the t-matrix and the r-matrix in the infinite volume scattering will also be included.

In Chapter 3, we will build a toy model. First we construct a Hamiltonian for $\sigma \to \pi\pi$ scattering, where π is a scalar meson which we use to investigate Lüscher's approach. We use the Hamiltonian to get the energy eigenvalues at certain lattice sizes. Then, the phase shifts at these energy eigenvalues can be acquired by Lüscher's formula. The exact infinite volume phase shifts can be calculated by evaluating the t-matrix or r-matrix. Thus, we can compare the finite volume phase shifts acquired by Lüscher's formula and the infinite volume phase shifts.

In Chapter 4, we are going to apply our techniques to the ρ decay in the real world. First we only consider the $\rho \to \pi\pi$ channel. Then we will include both the $\rho \to \pi\pi$ channel and the $\rho \to \omega\pi$ channel. We will compare the phase shifts obtained using Lüscher's formula with the exact infinite volume phase shifts.

Chapter 2

Theoretical Background

2.1 Overview

Atomic nuclei are composed of protons and neutrons. Protons and neutrons are in turn composed of quarks. In scattering processes, besides the proton and neutron, there are other resonances with higher energies which are also composed of quarks. The quarks in hadrons such as protons, neutrons, and other resonances, are governed by the strong interaction.

Quantum chromodynamics (QCD) is a theory which describes the strong interactions of the quarks. The strong interaction has a peculiar feature called asymptotic freedom. Quarks in a hadron are subject to the strong force which binds them together. The larger the distance between two quarks, the larger the energy associated with them. When quarks are close to each other, the strong force is reduced, as if they were free particles. When two quarks in a hadron get further away from each other, the force which binds them gets stronger, and it needs more energy to separate them further. If the energy becomes too large, the hadron becomes two, and a new pair of quarks appear, each of which reside in a hadron. Hence, the quarks are always found in hadrons and never observed in isolation. This is known as the color confinement.

In the high energy area, QCD can be studied perturbatively and analytically. However, in the low energy area, which is below about 1 GeV, the coupling constant

$$\alpha_s(k^2) \simeq \frac{1}{\beta_0 \ln(\frac{k^2}{\Lambda^2})}$$

becomes large, and QCD can not be studied perturbatively.[7] There still remains much to study for QCD in this region, for example, the identification of resonances in the low energy region.[8]

Lattice QCD is a technique to study the strong interaction non-perturbatively, and hence can be used to study QCD in the low energy regime.[9] By using lattice QCD and fitting techniques, the resonance masses have been extracted successfully from the pion scattering spectrum in the region $m_\pi^2 > 0.3GeV^2$.[10][11]. A lattice is a box of spacetime with finite volume specific boundary conditions. By using a lattice, the macroscopically continuous spacetime has been to be discretized. Hence, some finite volume effects would be introduced.[12][13][14][15][16]

Lattice QCD has proven very successful in studying low energy QCD. In addition, by twisting the boundary conditions, it can be used to study many specific aspects, such as multichannel scattering.[17] A problem for lattice QCD is that, when the lattice volume gets bigger, the required computational capacity increases drastically and becomes very demanding. Many methods have been used to tame the demand of the computational capacity, such as the quenched approximation, in which the sea quarks are ignored.[18] However, the computational cost is still a barrier which lattice QCD must face.

Besides the problem of computational cost, lattice QCD is subject to finite volume effects. For example, for a scattering process on a lattice, because of the finite volume and the imposed boundary conditions, the wave functions of the resonances as the intermediate states only allow certain discretized momentum values, and hence, certain discretized energy levels. However, a resonance in a scattering process in the real world does not correspond to any specific energy level in the lattice. We have to take the limit $L \to \infty$, which demands computational capacity.

For the low energy regime, M. Lüscher proposed a method to extract the scattering phase shifts of the waves from the discretized energy spectrum of a lattice. Lüscher's formalism can relate the scattering process in finite volume lattices with phase shifts in the infinite volume scattering in the real world. There is an inventory of literature about two-pion scattering with σ as the resonance in the intermediate state. However, investigations of Lüscher's formalism for different situations, such as other resonances, still need to be carried out. In this study we will look at $\sigma \to \pi\pi$ scattering first. Then, we will direct our investigation to $\rho \to \pi\pi$ scattering. In the latter case, the $\rho \to \pi\omega$ channel will also be considered.

In order to investigate Lüscher's formula, we have to set up a model of scattering on a lattice and calculate its energy spectrum. Then, we can use Lüscher's formula to get the phase shifts of the allowed energy levels. We will also compute the infinite volume scattering phase shifts, so that we can compare the phase shifts acquired from the finite volume lattice with those in the infinite volume case. So, in the following sections, we will start with the introduction of the setting and the construction of our scattering model.

2.2 Setting of Lattice

We first construct a toy model to investigate the scattering of two identical scalar mesons, for example, pions, in the center of mass frame. We will model this scattering process in a lattice of finite volume $L \times L \times L$ with periodic boundary conditions.

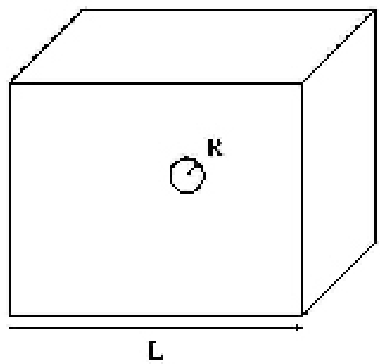

Fig. 2.2.1

The particle positions are $\mathbf{x}$, $\mathbf{y}$, and each particle has mass m_π, momentum k, energy W. We have

$$\mathbf{r} = \mathbf{x} - \mathbf{y}$$

$$k = \frac{2\pi}{L}|\mathbf{n}|, \ \mathbf{n} \in \mathbb{Z}^3$$

The energy of two non-interacting mesons is

$$W = 2m_\pi + \frac{k^2}{2\mu}$$

for non-relativistic case, where μ is the reduced mass, or

$$W = 2\sqrt{m_\pi^2 + k^2}$$

for the relativistic case. For now we take the non-relativistic case as we are interested in studying a matter of principle, not a realistic problem.

We limit our toy model to two pion elastic scattering:

$$W < 4m_\pi$$

with spin 0, i.e. scalar fields. We have $W < 4m_\pi$ instead of $W < 3m_\pi$ because G-parity forbids $\pi + \pi \to \pi + \pi + \pi$.

2.3 Constructing Hamiltonian

We will construct a Hamiltonian and use it to get the energy spectrum of the system on the lattice. In our toy model, we take a fictious σ meson as a resonance lying just above the two-pion threshold. This σ then dominates the low-energy $\pi-\pi$ scattering.

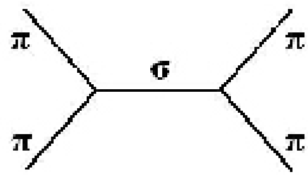

Fig. 2.1.2

Assume the interaction Lagrangian is

$$\mathcal{L}_{int} = g\sigma\pi^2$$

In this interaction Lagrangian, there is no derivative term, and we can construct the Hamiltonian as

$$H = H_0 + H_I$$

$$H_I = -L_I$$

We are going to construct H by finding the elements $\langle j \left| H \right| i \rangle$ where $|i\rangle$, $|j\rangle$ are the two-pion states.

In the center of mass frame and non-relativistic kinetics, suppose the momenta of the pions are $\mathbf{k}$ and $-\mathbf{k}$, then

$$H_0 \left| \sigma \right\rangle = m_{\sigma 0}$$

$$H_0 \left| \pi(\mathbf{k})\pi(-\mathbf{k}) \right\rangle = 2m_\pi + \frac{k^2}{2\mu}$$

where the reduced mass is

$$\mu = \frac{m_\pi}{2}$$

By periodic boundary condition of the lattice we must have $k = \frac{2\pi}{L}\left|\mathbf{n}\right|$, where $\mathbf{n} = (n_1, n_2, n_3)$, $n_1, n_2, n_3, |\mathbf{n}| \in \mathbb{N}$. Denote the allowed k's by k_i. k_q is just $\frac{2\pi}{L}q$, and we have

$$H_0 = \begin{pmatrix} m_{\sigma 0} & & & & & & \\ & 2m_\pi & & & & 0 & \\ & & 2m_\pi + \frac{k_1^2}{m_\pi} & & & & \\ & & & 2m_\pi + \frac{k_2^2}{m_\pi} & & & \\ & & & & 2m_\pi + \frac{2k_3^2}{m_\pi} & & \\ & 0 & & & & 2m_\pi + \frac{2k_4^2}{m_\pi} & \\ & & & & & & \ddots \end{pmatrix}$$

where $m_{\sigma 0}$ is the bare mass of σ.

The interaction part of the Hamiltonian is

$$H_I = \begin{pmatrix} 0 & g(k_0) & g(k_1) & g(k_2) & g(k_3) & g(k_4) & \cdots \\ g(k_0) & & & & & & \\ g(k_1) & & & & & & \\ g(k_2) & & & & & & \\ g(k_3) & & & & 0 & & \\ g(k_4) & & & & & & \\ \vdots & & & & & & \end{pmatrix}$$

and the allowed values of k are

$$k = \frac{2\pi}{L} q$$

where $q = |\mathbf{n}|$. So we have $q_0 = 0$ for k_0, $q_1 = 1$ for k_1, $q_2 = 2$ for k_2, etc. However, for k_1, there are six corresponding pairs of $\mathbf{n}$'s for the center of mass coordinates coming in three pairs, namely {{0, 0, 1}, {0, 0, -1}}, {{0, 1, 0}, {0, -1, 0}}, {{1, 0, 0}, {-1, 0, 0}}. Hence, we will have three rows and columns corresponding to k_1 in H_I. To make H_I more compact, we can re-weight each k_n according to the number of corresponding $\mathbf{n}$'s.

The re-weighted interaction Hamiltonian is

$$H_I = \begin{pmatrix} 0 & \sqrt{C_0}g(k_0) & \sqrt{C_1}g(k_1) & \sqrt{C_2}g(k_2) & \sqrt{C_3}g(k_3) & \sqrt{C_4}g(k_4) & \cdots \\ \sqrt{C_0}g(k_0) & & & & & & \\ \sqrt{C_1}g(k_1) & & & & & & \\ \sqrt{C_2}g(k_2) & & & & & & \\ \sqrt{C_3}g(k_3) & & & & 0 & & \\ \sqrt{C_4}g(k_4) & & & & & & \\ \vdots & & & & & & \end{pmatrix}$$

where $g(k_q)$ is the coupling constant and C_q is the number of distinct 3-D vectors $\mathbf{n} = (n_1, n_2, n_3)$ where $n_1, n_2, n_3, |\mathbf{n}| \in \mathbb{Z}$ and $|\mathbf{n}| = q$. Then, the full Hamiltonian is

$$
H = \begin{pmatrix}
m_{\sigma 0} & \sqrt{C_0}g(k_0) & \sqrt{C_1}g(k_1) & \sqrt{C_2}g(k_2) & \sqrt{C_3}g(k_3) & \sqrt{C_4}g(k_4) & \cdots \\
\sqrt{C_0}g(k_0) & 2m_\pi & & & & & \\
\sqrt{C_1}g(k_1) & & 2m_\pi + \frac{k_1^2}{m_\pi} & & & & \\
\sqrt{C_2}g(k_2) & & & 2m_\pi + \frac{k_2^2}{m_\pi} & & & \\
\sqrt{C_3}g(k_3) & & & & 2m_\pi + \frac{2k_3^2}{m_\pi} & & \\
\sqrt{C_4}g(k_4) & & & & & 2m_\pi + \frac{2k_4^2}{m_\pi} & \\
\vdots & & & & & & \ddots
\end{pmatrix}
$$

It is then straightforward to extract the energy eigenvalues W_1, W_2, W_3... of the full Hamiltonian H at different lattice sizes.

2.4 Avoided Level Crossing

If there is no interaction, the full Hamiltonian is just H_0, and the energy eigenvalues are just $m_\sigma, 2m_\pi, 2m_\pi + \frac{2k_i^2}{m_\pi}$. An example of the relation between energy eigenvalues and L can be seen from Fig. 2.4.1.

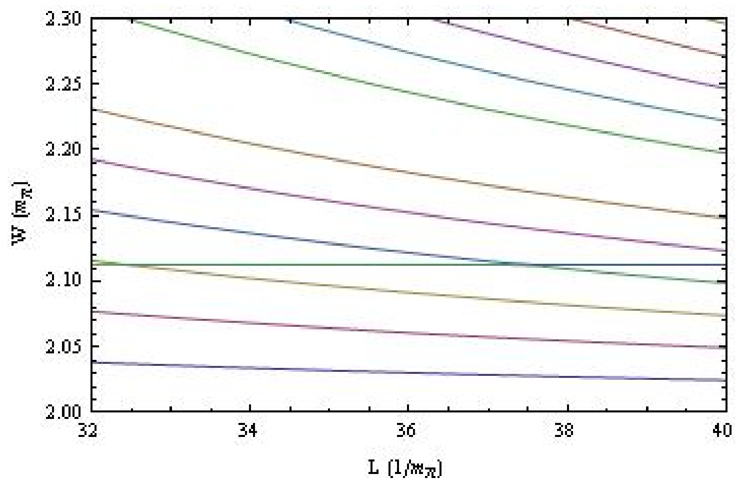

Fig. 2.4.1 An example of the energy spectrum (in units of m_π) with no interaction

When the interaction is turned on, the full Hamiltonian is $H_0 + H_I$, and the relation between energy eigenvalues and L becomes what are displayed in Fig. 2.4.2.

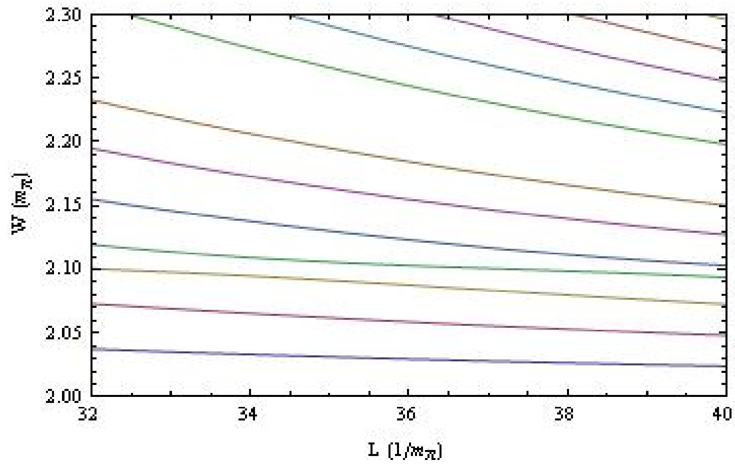

Fig. 2.4.2 An example of energy
spectrum (in units of m_π) with interaction

The eigenvalues of H will exhibit the phenomenon of avoided level crossing. This phenomenon makes extracting resonance masses more complicated.[19]

2.5 Lüscher's Formalism

In this section we are going to review Lüscher's formalism based on his papers.[20][21]

Lüscher's formalism relates the scattering phase shift, δ, of the infinite volume case in the real world to the momentum, k, and hence length, L, of the finite volume lattice model.

We are looking at the low energy regime, so we begin with a non-relativistic toy model. The Hamiltonian operator in this case is

$$H = -\frac{1}{2\mu} \bigtriangledown^2 + V(r)$$

The Hamiltonian above is an elliptic operator. The elliptic regularity implies that any locally square integrable, i.e. normalizable, solution $\Psi(r)$ of the Schrödinger equation

$$H\Psi = E\Psi$$

is smooth. Hence, the expansion of $\Psi(r)$ in spherical harmonics

$$\psi(\mathbf{r}) = \sum_{l=0}^{\infty} \sum_{m=-l}^{l} Y_{lm}(\theta, \phi) \Psi_{lm}(r)$$

converges rapidly, i.e. the deviation of $\Psi_{lm}(r)$ from $j_l(kr)$ approaches 0 as $l \to \infty$, where $\Psi_{lm}(r)$ are smooth solutions of the radial Schrödinger equation

$$(\frac{d^2}{dr^2} + \frac{2}{r}\frac{d}{dr} - \frac{l(l+1)}{r^2} + k^2 - 2\mu V(r))\Psi_{lm}(r) = 0$$

Because of the potential, the total mass of a two-body system may be less than the sum of the mass of each particle. For example, in a hydrogen atom, which is composed of a proton and an electron, we have

$$m_H < m_p + m_e$$

So for two identical particles, we could have $W < 2m$, and in this case by

$$W = 2\sqrt{m^2 + k^2}$$

we have a pure imaginary momentum k. For the present case, we are looking at scattering above threshold, so we only consider real k's.

Let $u_l(r,k)$ be solutions of the radial Schrödinger equation, for r near the origin, we have

$$\lim_{r\to 0} r^{-l} u_l(r,k) = \text{constant}$$

and

$$\Psi_{lm}(r) = b_{lm} u_l(r,k)$$

for some constants b_{lm}.

In the region where the potential is small, i.e. $r > R$, the solution $u_l(r,k)$ of the radial Schrödinger equation is a combination of two linearly independent spherical Bessel functions $j_l(kr)$ and $n_l(kr)$:

$$u_l(r,k) = \alpha_l(k) j_l(kr) + \beta_l(k) n_l(kr)$$

where α_l, β_l are constants and

$$\alpha_l^*(k) = \alpha_l(k^*)$$

$$\beta_l^*(k) = \beta_l(k^*)$$

$$\alpha_l(-k) = -\alpha_l(k)$$

$$\beta_l(-k) = -\beta_l(k)$$

For real $k > 0$ and angular momentum l,

$$e^{2i\delta_l(k)} = \frac{\alpha_l(k) + i\beta_l(k)}{\alpha_l(k) - i\beta_l(k)} \tag{2.5.1}$$

where $\delta_l(k)$ is the phase shift in the sense that it is the shift in the phase of the wave function in the region where the potential $V = 0$ caused by the interaction.

$\Psi(\mathbf{r})$ is called a singular periodic solution of the Helmholtz equation

$$(\bigtriangledown^2 + k^2)\Psi(\mathbf{r}) = 0$$

if

(i) $\Psi(\mathbf{r})$ is a smooth function defined for all $\mathbf{r} \neq 0 \pmod L$.
(ii) $\Psi(\mathbf{r})$ satisfies the Helmholtz equation.
(iii) $\Psi(\mathbf{r})$ is periodic with period L.
(iv) near $r = 0$, $\Psi(\mathbf{r})$ is bounded by $\frac{1}{r}$, i.e.

$$\sup_{0<r<\frac{L}{2}} \left| r^{\Lambda+1}\Psi(\mathbf{r}) \right| < \infty, \ \Lambda \in \mathbb{Z}$$

All other solutions can be constructed from these singular periodic solutions.

Since the expansion of $\Psi(\mathbf{r})$ converges rapidly as l increases, we can introduce an angular momentum cutoff at $l = \Lambda$.

Since the Green function has the form

$$G(\mathbf{r}, k^2) = L^{-3} \sum_{\mathbf{p}} \frac{e^{i\mathbf{pr}}}{\mathbf{p}^2 - k^2}$$

where $\mathbf{p} = \frac{2\pi}{L}\mathbf{n}$, $n \in \mathbb{Z}^3$. We discuss the solution $\Psi(\mathbf{r})$ of the Helmholtz equation in two cases: the case where $k \in R$, $k \neq \frac{2\pi}{L}|\mathbf{n}|$, $\mathbf{n} \in \mathbb{Z}^3$ and the case where $k \in R$, $k = \frac{2\pi}{L}|\mathbf{n}|$, $\mathbf{n} \in \mathbb{Z}^3$.

In the region where the potential $V(r) = 0$, the Schrödinger equation becomes the Helmholtz equation. The Helmholtz equation in spherical coordinates can be solved by separation of variables as a product of the radial part and the angular part.[22] As shown in [20], because of the non-spherical boundary conditions, for $k \in R$, $k \neq \frac{2\pi}{L}|\mathbf{n}|$, $\mathbf{n} \in \mathbb{Z}^3$, in the solutions of the Helmholtz equation with angular momentum cutoff of two particle scattering can be written as

$$\Psi(\mathbf{r}) = \sum_{l=0}^{\Lambda}\sum_{m=-l}^{l} v_{lm}\frac{(-1)^l}{4\pi}k^{l+1}(Y_{lm}(\theta,\phi)n_l(kr) + \sum_{l'=0}^{\infty}\sum_{m'=-l'}^{l'} \mathcal{M}_{lm,l'm'}Y_{l'm'}(\theta,\phi)j_{l'}(kr)) \tag{2.5.2}$$

And by expansion of $\Psi(r)$ in products of spherical harmonics and $\Psi_{lm}(r)$, we have

$$\begin{aligned} \Psi(\mathbf{r}) &= \sum_{l=0}^{\infty}\sum_{m=-l}^{l} Y_{lm}(\theta,\phi)\Psi_{lm}(r) \\ &= \sum_{l=0}^{\infty}\sum_{m=-l}^{l} Y_{lm}(\theta,\phi)b_{lm}(\alpha_l(k)j_l(kr) + \beta_l(k)kn_l(kr)) \end{aligned} \tag{2.5.3}$$

Since (2.5.2)=(2.5.3) , by comparing the $j_l(kr)$ part, we have

$$\sum_{l=0}^{\infty}\sum_{m=-l}^{l} Y_{lm}(\theta,\phi)b_{lm}\alpha_l(k)j_l(kr) = \sum_{l=0}^{\Lambda}\sum_{m=-l}^{l} v_{lm}\frac{(-1)^l}{4\pi}k^{l+1}\sum_{l'=0}^{\infty}\sum_{m'=-l'}^{l'}\mathcal{M}_{lm,l'm'}Y_{l'm'}(\theta,\phi)j_{l'}(kr)$$

where

$$\mathcal{M}_{lm,l'm'} = \frac{(-1)^l}{4\pi}k^{l+1}\sum_{j=|l-l'|}^{l+l'}\sum_{s=-j}^{j}\frac{i^j}{q^{j+1}}\mathcal{Z}_{js}(1,q^2)C_{lm,js,l'm'}$$

with $\mathcal{Z}_{js}(1,q^2)$ being the zeta function and $C_{lm,js,l'm'}$ being related to the Wigner 3j-symbols through

$$C_{lm,js,l'm'} = (-1)^{m'}i^{l-j+l'}\sqrt{(2l+1)(2j+1)(2l'+1)}\begin{pmatrix} l & j & l' \\ 0 & 0 & 0 \end{pmatrix}\begin{pmatrix} l & j & l' \\ m & s & -m' \end{pmatrix}$$

By cubic symmetry in $\mathcal{M}_{lm,l'm'}$, it becomes

$$\sum_{l=0}^{\infty}\sum_{m=-l}^{l} Y_{lm}(\theta,\phi)b_{lm}\alpha_l(k)j_l(kr) = \sum_{l'=0}^{\Lambda}\sum_{m'=-l'}^{l'} v_{l'm'}\frac{(-1)^{l'}}{4\pi}k^{l'+1}\sum_{l=0}^{\infty}\sum_{m=-l}^{l}\mathcal{M}_{l'm',lm}Y_{lm}(\theta,\phi)j_l(kr) \tag{2.5.4}$$

By comparing the $j_l(kr)$ part we have

$$b_{lm}\alpha_l(k) = \sum_{l'=0}^{\Lambda}\sum_{m'=-l'}^{l'} v_{l'm'}\frac{(-1)^{l'}}{4\pi}k^{l'+1}\mathcal{M}_{l'm',lm} \tag{2.5.5}$$

By comparing the $n_l(kr)$ part we have

$$\sum_{l=0}^{\infty}\sum_{m=-l}^{l} Y_{lm}(\theta,\phi)b_{lm}\beta_l(k)n_l(kr) = \sum_{l=0}^{\Lambda}\sum_{m=-l}^{l} v_{lm}\frac{(-1)^l}{4\pi}k^{l+1}Y_{lm}(\theta,\phi)n_l(kr)$$

and hence

$$b_{lm}\beta_l(k) = v_{lm}\frac{(-1)^l}{4\pi}k^{l+1}$$

so

$$v_{lm} = b_{lm}\beta_l(k)\frac{4\pi}{(-1)^l k^{l+1}} \tag{2.5.6}$$

for $l < \Lambda$. Put v_{lm} of (2.5.6) into (2.5.5) we have

$$b_{lm}\alpha_l(k) = \sum_{l'=0}^{\Lambda}\sum_{m'=-l'}^{l'} b_{l'm'}\beta_{l'}(k)\mathcal{M}_{l'm',lm}$$

Move the right hand side to the left we have

$$b_{lm}\alpha_l(k) - \sum_{l'=0}^{\Lambda}\sum_{m'=-l'}^{l'} b_{l'm'}\beta_{l'}(k)\mathcal{M}_{l'm',lm} = 0 \tag{2.5.7}$$

Hence we have a system of homogeneous linear equations for the coefficients b_{lm}. For b_{lm}, l can be from 0 to Λ. So the number of equations equals the number of variables. Since it is a homogenerous system, $b_{lm} = 0$ must be its solution, unless the associated determinant of the linear equation system is zero. So the problem is to find values of k corresponding to the eigenvalues of the Hamiltonian with introduced angular momentum cutoff such that the associated determinant of the linear equation system of (2.5.7) becomes zero.

We can define linear operators

$$[Mv_{l'm'}]_{lm} = \mathcal{M}_{l'm',lm}$$

$$[Av]_{lm} = \alpha_l(k)v_{lm}$$

$$[Bv]_{lm} = \beta_l(k)v_{lm}$$

Then from (2.5.1) we have

$$e^{2i\delta} = \frac{A+iB}{A-iB}$$

The associated determinant of the linear equation system of (2.5.7) becomes $\det(A-BM)$. In order to have non-zero solutions for b_{lm}, the associated determinant has to be

$$\det(A-BM) = 0$$

In the case where k is real, since $\mathcal{M}$ is Hermitian and since the eigenvalues of $A-iB$ do not vanish, we have

$$\det((A-iB)(M-i)) \neq 0$$

So we have

$$\det(A-BM) = \det((A-BM)\frac{(A-iB)(M-i)}{(A-iB)(M-i)}) = 0$$

$$\Rightarrow \det((-2i)(A-BM)\frac{(A-iB)(M-i)}{(A-iB)(M-i)}) = 0$$

$$\det(\frac{-2i(A-BM)}{(A-iB)(M-i)}) = 0$$

$$\det(\frac{AM-iA+iBM+B-AM-iA+iBM-B}{(A-iB)(M-i)}) = 0$$

$$\det\left(\frac{(A+iB)(M-i)-(A-iB)(M+i)}{(A-iB)(M-i)}\right)=0$$

$$\det\left(\frac{A+iB}{A-iB}-\frac{M+i}{M-i}\right)=0$$

$$\Rightarrow \det(e^{2i\delta}-U)=0 \tag{2.5.8}$$

where

$$U=\frac{M+i}{M-i}$$

For $k \in R$, $k=\frac{2\pi}{L}|\mathbf{n}|$, $\mathbf{n} \in \mathbb{Z}^3$, let $\mathbf{p}$ be any of these special values of $\mathbf{k}$, then the solutions of the Helmholtz equation with angular momentum cutoff of two particle scattering can be written as

$$\Psi(\mathbf{r})=4\pi\sum_{\mathbf{p}} w_p \sum_{l=0}^{\infty}\sum_{m=-l}^{l} i^l Y_{lm}^*(\theta_p,\phi_p)Y_{lm}(\theta,\phi)j_l(pr)$$

$$+\sum_{l=0}^{\Lambda}\sum_{m=-l}^{l} v_{lm}\frac{(-1)^l}{4\pi}k^{l+1}(Y_{lm}(\theta,\phi)n_l(kr)+\sum_{l'=0}^{\infty}\sum_{m'=-l'}^{l'}\mathcal{M}'_{lm,l'm'}Y_{l'm'}(\theta,\phi)j_{l'}(kr))$$

where

$$\mathcal{M}_{lm,l'm'}=\lim_{q\to|\mathbf{n}|}\frac{1}{q^2-\mathbf{n}^2}(-\frac{2}{\pi|\mathbf{n}|}\sum_{\mathbf{p}} i^{l-l'}Y_{lm}^*(\theta_p,\phi_p)Y_{lm}(\theta_p,\phi_p))+\mathcal{M}'_{lm,l'm'}+\mathcal{O}(q^2-\mathbf{n}^2)$$

With cubic symmetry, it becomes

$$\Psi(\mathbf{r})=4\pi\sum_{\mathbf{p}} w_p \sum_{l'=0}^{\infty}\sum_{m'=-l'}^{l'} i^{l'} Y_{l'm'}^*(\theta_p,\phi_p)Y_{l'm'}(\theta,\phi)j_{l'}(pr)$$

$$+\sum_{l'=0}^{\Lambda}\sum_{m'=-l'}^{l'} v_{l'm'}\frac{(-1)^{l'}}{4\pi}k^{l'+1}(Y_{l'm'}(\theta,\phi)n_{l'}(kr)+\sum_{l=0}^{\infty}\sum_{m=-l}^{l}\mathcal{M}'_{l'm',lm}Y_{lm}(\theta,\phi)j_l(kr)) \tag{2.5.9}$$

By comparing the $j_l(kr)$ part of (2.5.3) and (2.5.9), we have

$$b_{lm}\alpha_l(k)=4\pi\sum_{\mathbf{p}} w_p\sum_{l'=0}^{\infty}\sum_{m'=-l'}^{l'} i^{l'}Y_{l'm'}^*(\theta_p,\phi_p)+\sum_{l'=0}^{\Lambda}\sum_{m'=-l'}^{l'} v_{l'm'}\frac{(-1)^{l'}}{4\pi}k^{l'+1}\mathcal{M}'_{l'm',lm} \tag{2.5.10}$$

By comparing the $n_l(kr)$ part of (2.5.3) and (2.5.9), we have

$$b_{lm}\beta_l(k) = v_{lm}\frac{(-1)^l}{4\pi}k^{l+1}$$

If we set $b_{lm} = 0$ and $v_{lm} = 0$, then by (2.5.10)

$$4\pi \sum_{\mathbf{p}} w_p \sum_{l'=0}^{\infty} \sum_{m'=-l'}^{l'} i^{l'} Y^*_{l'm'}(\theta_p, \phi_p) = 0$$

There will be no solutions for a fixed k since the number of spherical harmonics is larger than the number of p's. When $b_{lm} \neq 0$, there are further solutions if and only if

$$\lim_{q\to|\mathbf{n}|} \det(e^{2i\delta} - U) = 0$$

which can be seen as a special case of (2.5.8). So now we have considered all real k's.

If the spherical component of a smooth periodic solution of the Helmholtz equation for $\Psi(\mathbf{r})$ can be written as

$$\Psi_{lm}(r) = b_{lm}(\alpha_l(k)j_l(kr) + \beta_l(k)n_l(kr))$$

i.e. such b_{lm} exists in the region $R < r < \frac{L}{2}$, then there exists a unique eigenfunction of the Hamiltonian H which coincides with $\Psi(\mathbf{r})$ in the region $R < r < \frac{L}{2}$. Hence, eigenfunctions of H can be related with $\alpha_l(k)$ and $\beta_l(k)$, and from (2.5.1) the energy spectrum of an energy interval is calculable when the scattering phase shifts in that energy interval are known.

In our simple model, we have $k = \frac{2\pi}{L}|\mathbf{n}|$ by the periodic boundary conditions of the lattice and consider the S wave case. In the case of S wave, where the quantum number l is equal to 0, the homogeneous linear equation system is reduced to one equation, and the dimension of the matrix $e^{2i\delta} - U$ is reduced to 1×1. Hence

$$e^{2i\delta_0} - \frac{m_{00} + i}{m_{00} - i} = 0$$

where m_{00} is the matrix element of M in this case.

Let $\phi(q)$ be a function such that

$$\frac{m_{00} + i}{m_{00} - i} = e^{-2i\phi(q)}$$

Then we have Lüscher's formalism

$$e^{2i\delta_0(k)} = \frac{m_{00}+i}{m_{00}-i} = e^{-2i\phi(q)} \tag{2.5.11}$$

where

$$\phi(0) = 0$$

$$q = \frac{kL}{2\pi} = |\mathbf{n}|$$

$$m_{00} = \frac{1}{\pi^{3/2} q} \mathcal{Z}_{00}(1, q^2)$$

and $\mathcal{Z}_{00}(1, q^2)$ is the zeta function at $j = 0$, $s = 0$, namely:

$$\mathcal{Z}_{00}(1, q^2) = \frac{1}{\sqrt{4\pi}} \sum_{\mathbf{n}\in\mathbb{Z}^3} \frac{1}{\mathbf{n}^2 - q^2}$$

And we have

$$\tan\phi(q) = -\frac{\pi^{\frac{3}{2}} q}{\mathcal{Z}_{00}(1, q^2)}$$

We need to calculate $\mathcal{Z}_{00}(1, q^2)$. $\mathcal{Z}_{00}(1, q^2)$ has infinities when $\mathbf{n}^2 = q^2$, and we need to remove the infinities, i.e. regularize it. We can write

$$\begin{aligned}
\frac{1}{n^2 - q^2} &= \frac{1}{n^2 - q^2} - \frac{1}{n^2} + \frac{1}{n^2} \\
&= \frac{n^2 - (n^2 - q^2)}{n^2(n^2 - q^2)} + \frac{1}{n^2} \\
&= \frac{q^2}{n^4(n^2 - q^2)} + \frac{1}{n^2} - \frac{q^2}{n^4} + \frac{q^2}{n^4} \\
&= \frac{n^2 q^2 - q^2(n^2 q^2)}{n^4(n^2 - q^2)} + \frac{1}{n^2} + \frac{q^2}{n^4} \\
&= \frac{q^4}{n^4(n^2 - q^2)} + \frac{1}{n^2} + \frac{q^2}{n^4}
\end{aligned}$$

Let $N = n^2$, we have

$$\frac{1}{n^2 - q^2} = \frac{q^4}{N^2(N - q^2)} + \frac{1}{N} + \frac{q^2}{N^2}$$

Because we are summing over $\mathbf{n} \in \mathbb{Z}^3$, the terms involving $N = n^2$ should be weighed by C_n as in Section 2.3. Hence we have

$$\sum_{\mathbf{n}\in\mathbb{Z}^3} \frac{1}{\mathbf{n}^2 - q^2} = -\frac{1}{q^2} + \sum_{N=1}^{\infty} C_N \left(\frac{q^4}{N^2(N - q^2)} + \frac{1}{N} + \frac{q^2}{N^2}\right)$$

which can be written as[20]

$$\mathcal{Z}_{00}(1,q^2) = \frac{1}{\sqrt{4\pi}}(-\frac{1}{q^2} + J_0 + J_1 q^2 + \sum_{N=1}^{\infty} C_N \frac{q^4}{N^2(N-q^2)})$$

where $J_0 = -8.91363292$ and $J_1 = 16.53231596$

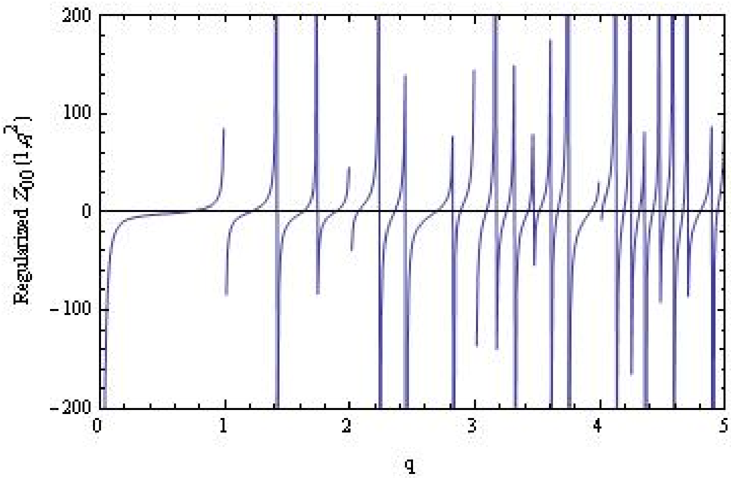

Fig. 2.5.1 Regularized $\mathcal{Z}_{00}(1,q^2)$ function

$\phi(q)$ can be obtained from $\mathcal{Z}_{00}(1,q^2)$ with an adjustment. The adjustment arises from the periodicity of the tan function and does not effect Lüscher's formula. This adjustment will be introduced in Section 2.7.

2.6 Infinite Volume Phase Shift

Now we turn to the phase shift for scattering in infinite volume. We assume the interaction Lagrangian as

$$\mathcal{L}_{int} = g(k)\sigma\pi^2$$

and potential operator in the form

$$v = \frac{g(k)g(k')}{E - (m_\sigma - 2m_\pi)}$$

The corresponding Lippmann-Schwinger equation is

$$t = v + vGt$$

where t is the t-matrix.

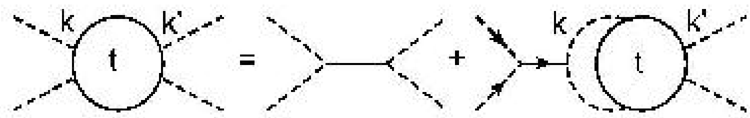

Fig. 2.6.1 Schematic diagram of the t-matrix

The t-matrix has the general form

$$t(k,k';E^+) = g(k)g(k')\tau(E^+) \tag{2.6.1}$$

where

$$E^+ = \frac{k_0^{2+}}{2m} = \lim_{\eta\to 0}(\frac{k_0^2}{2m} + i\eta)$$

When momenta are written in vector,

$$t_l(\mathbf{k},\mathbf{k}';\frac{k_0^{2+}}{2m}) = v(\mathbf{k},\mathbf{k}_0) + \int d^3k'k'^2\frac{v_l(\mathbf{k},\mathbf{k}')t_l(\mathbf{k}',\mathbf{k}_0;\frac{k_0^{2+}}{2m})}{\frac{k_0^2}{2m}+i\eta-\frac{k'^2}{2m}}$$

Let us separate the directions and magnitudes of momenta, so that we have

$$\sum_{l,m} Y_{lm}(\hat{\mathbf{k}})Y_{lm}^*(\hat{\mathbf{k}}_0)t_l(k,k_0;\tfrac{k_0^{2+}}{2m}) = \sum_{l,m} Y_{lm}(\hat{\mathbf{k}})Y_{lm}^*(\hat{\mathbf{k}}_0)v_l(k,k_0)$$

$$+\sum_{l,m,l',m'}\int_0^\infty dk'k'^2 Y_{lm}(\hat{\mathbf{k}})Y_{l'm'}^*(\hat{\mathbf{k}}_0)\int d\hat{k}Y_{lm}^*(\hat{\mathbf{k}}')Y_{l'm'}(\hat{\mathbf{k}}')\frac{v_l(k,k')t_l(k',k_0;\frac{k_0^{2+}}{2m})}{\frac{k_0^2}{2m}+i\eta-\frac{k'^2}{2m}}$$

Using the orthonormality of the spherical harmonics, we find:

$$t_l(k,k_0;\frac{k_0^{2+}}{2m}) = v_l(k,k_0) + \int_0^\infty dk'k'^2\frac{v_l(k,k')t_l(k',k_0;\frac{k_0^{2+}}{2m})}{\frac{k_0^2}{2m}+i\eta-\frac{k'^2}{2m}}$$

Substitute t_l and v_l by $t(k,k';E^+) = g(k)g(k')\tau(E^+)$ and $v = \frac{g(k)g(k')}{E-(m_{\sigma 0}-2m_\pi)}$ and replace m by μ we have

$$g(k)g(k)\tau(E^+) = \frac{g(k)g(k)}{E+2m_\pi-m_{\sigma 0}} + \int_0^\infty \frac{dk'k'^2g(k)g(k')}{E+2m_\pi-m_{\sigma 0}}\frac{g(k')g(k)\tau(E^+)}{E-\frac{k'^2}{2\mu}+i\eta}$$

$$\tau(\frac{k_0^{2+}}{2\mu}) = \frac{1}{E+2m_\pi-m_{\sigma 0}} + \int_0^\infty \frac{1}{E+2m_\pi-m_{\sigma 0}}\frac{dk'k'^2g^2(k')\tau(\frac{k_0^{2+}}{2\mu})}{E-\frac{k'^2}{2\mu}+i\eta}$$

$$\tau(\frac{k_0^{2+}}{2\mu})(1-\int_0^\infty \frac{1}{E+2m_\pi-m_{\sigma0}}\frac{dk'k'^2g^2(k')}{E^+-\frac{k'^2}{2\mu}+i\eta})=\frac{1}{E+2m_\pi-m_{\sigma0}}$$

$$\tau(\frac{k_0^{2+}}{2\mu})=\frac{1}{E^++2m_\pi-m_{\sigma0}-\int_0^\infty \frac{dk'k'^2g^2(k')}{E^+-\frac{k'^2}{2\mu}+i\eta}}$$

$$\Rightarrow\ \tau(\frac{k_0^{2+}}{2\mu})=\frac{1}{\frac{k_0^2}{2\mu}+2m_\pi-m_{\sigma0}-2\mu\int_0^\infty \frac{dk'k'^2g^2(k')}{k_0^2-k'^2+i\eta}}$$

Hence we have

$$t_l(k,k;\frac{k_0^{2+}}{2\mu})=\frac{g^2(k)}{\frac{k_0^2}{2\mu}+2m_\pi-m_{\sigma0}-2\mu\int_0^\infty \frac{dk'k'^2g^2(k')}{k_0^2-k'^2+i\eta}} \tag{2.6.2}$$

Now we look at the relation between the t matrix and the r matrix. In operator form, from

$$r(E)=v+vG_0^P(E)r(E) \tag{2.6.3}$$

where G_0^P means adopting the Cauchy principal value of the Green's function in G_0, and from

$$t(E^+)=v+vG_0(E^+)t(E^+) \tag{2.6.4}$$

if we multiply (2.6.3) by v^{-1} on the left and r^{-1} on the right, we have

$$v^{-1}=r^{-1}+G_0^P(E)$$

and if we multiply (2.6.4) by v^{-1} on the left and t^{-1} on the right, we have

$$v^{-1}=t^{-1}(E^+)+G_0(E^+)$$

So we have

$$t^{-1}(E^+)=r^{-1}(E)+(G_0^P(E)-G_0(E^+))$$

$$t(E^+)=r(E)+r(E)(G_o(E^+)-G_0^P(E))t(E^+)$$

By Sokhatsky–Weierstrass theorem,

$$\lim_{\eta\to0}\int_a^b \frac{f(x)dx}{x-c\pm i\eta}=P\int_a^b\frac{f(x)dx}{x-c}\mp i\pi\int_a^b f(x)\delta(x-c)dx$$

where $a<c<b$. Hence

$$t_l(k,k_0;E^+)=r_l(k,k_0;E)-i\pi\int_0^\infty dk'k'^2r_l(k,k';E)\delta(E-\frac{k'^2}{2m})t_l(k',k_0;E^+)$$

Let

$$E = \frac{k_E^2}{2m}$$

Then by

$$\begin{aligned}\delta(E - \frac{k'^2}{2m}) &= \delta(\frac{(k_E + k')(k_E - k')}{2m}) \\ &= \frac{m}{k_E}\delta(k_E - k')\end{aligned}$$

we have

$$t_l(k, k_0; E^+) = r_l(k, k_0; E) - i\pi m k_E r_l(k, k_E; E) t_l(k_E, k_0; E^+) \tag{2.6.5}$$

Let $k = k_E$ in (2.6.5), we have

$$t_l(k_E, k_0; E^+) = r_l(k_E, k_0; E) - i\pi m k_E r_l(k_E, k_E; E) t_l(k_E, k_0; E^+)$$

$$t_l(k_E, k_0; E^+)(1 + i\pi m k_E r_l(k_E, k_E; E)) = r_l(k_E, k_0; E)$$

$$\Rightarrow \; t_l(k_E, k_0; E^+) = \frac{r_l(k_E, k_0; E)}{1 + i\pi m k_E r_l(k_E, k_E; E)}$$

For elastic scattering, we need $t_l(k_E, k_E; \frac{k_E^{2+}}{2m})$ and $r_l(k_E, k_E; \frac{k_E^{2+}}{2m})$, so we set k_0 as k in $t_l(k_E, k_0; E^+)$ and $r_l(k_E, k_0; E)$ to get $t_l(k_E, k_E; \frac{k_E^{2+}}{2m})$ and $r_l(k_E, k_E; \frac{k_E^{2+}}{2m})$. For convenience, let

$$x = -\pi m k_E$$

Then we have

$$t_l(k_E, k_E; E^+) = \frac{r_l(k_E, k_E; E)}{1 - ixr_l(k_E, k_E; E)}$$

$$\frac{xt_l(k_E, k_E; E^+)}{xr_l(k_E, k_E; E)} = \frac{1}{1 - ixr_l(k_E, k_E; E)}$$

$$|1 - ixr_l(k_E, k_E; E)| \frac{xt_l(k_E, k_E; E^+)}{xr_l(k_E, k_E; E)} = \frac{1 + ixr_l(k_E, k_E; E)}{|1 + ixr_l(k_E, k_E; E)|}$$

Let

$$\frac{1 + ixr_l(k_E, k_E; E)}{|1 + ixr_l(k_E, k_E; E)|} = \cos\delta_l + i\sin\delta_l$$

where δ_l is real and called the phase shift. Then

$$\sin\delta_l = \frac{xr_l(k_E, k_E; E)}{|1 + ixr_l(k_E, k_E; E)|}$$

$$\cos\delta_l = \frac{1}{|1 + ixr_l(k_E, k_E; E)|}$$

Then we have

$$xt_l(k_E, k_E; \frac{k_E^{2+}}{2m}) = e^{i\delta_l}\sin\delta_l$$

$$\Rightarrow \; t_l(k_E, k_E; \frac{k_E^{2+}}{2m}) = -\frac{e^{i\delta_l}\sin\delta_l}{\pi m k_E} \tag{2.6.6}$$

and

$$\Rightarrow \; r_l(k_E, k_E; \frac{k_E^{2}}{2m}) = -\frac{\tan\delta_l}{\pi m k_E} \tag{2.6.7}$$

From (2.6.2) and (2.6.6) we have

$$\frac{g^2(k)}{\frac{k_0^2}{2\mu} + 2m_\pi - m_{\sigma 0} - 2\mu\int_0^\infty \frac{dk' k'^2 g^2(k')}{k_0^2 - k'^2 + i\eta}} = t_l(k, k; \frac{k_0^{2+}}{2\mu}) = -\frac{e^{i\delta_l}\sin\delta_l}{\pi m_\pi k_0}$$

Similarly from (2.6.3) we have

$$r_l(k, k; \frac{k_0^2}{2\mu}) = \frac{g^2(k)}{\frac{k_0^2}{2\mu} + 2m_\pi - m_{\sigma 0} - 2\mu P\int_0^\infty \frac{dk' k'^2 g^2(k')}{k_0^2 - k'^2 + i\eta}} \tag{2.6.8}$$

From (2.6.7) and (2.6.8) we have

$$\frac{g^2(k)}{\frac{k_0^2}{2\mu} + 2m_\pi - m_{\sigma 0} - 2\mu P\int_0^\infty \frac{dk' k'^2 g^2(k')}{k_0^2 - k'^2 + i\eta}} = r_l(k, k; \frac{k_0^2}{2\mu}) = -\frac{\tan\delta_l}{\pi \mu k_0} \tag{2.6.9}$$

An alternative way is that the r matrix has the general form

$$r(k, k'; E) = g(k)g(k')\rho(E)$$

and by applying the same method of derivation of t-matrix from (2.6.1) to (2.6.2) on r-matrix we can also find (2.6.9).

By (2.6.9), we can calculate the infinite volume phase shifts for $\pi\pi$ scattering through the coupling to the σ with its bare mass, $m_{\sigma 0}$, chosen to yield a dressed pole position at $E = 2.1$ (m_π).

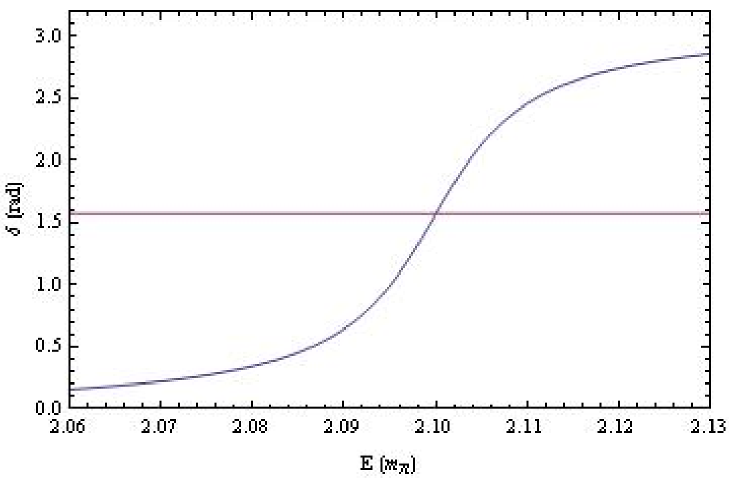

Fig. 2.6.2 Infinite volume phase shift

2.7 Finite Volume Phase Shift

Lüscher's formula relates the infinite volume phase shifts to the energy eigenvalues of the finite volume scattering problem. For $l = 0$ case, from (2.5.11),

$$e^{2i\delta_0(k)} = \frac{m_{00} + i}{m_{00} - i} = e^{-2i\phi(q)}$$

where $\delta_0(k)$ is the phase shifts. Then

$$\phi(q) = r\pi - \delta_0(k), r \in \mathbb{N}$$

$\phi(q)$ is a continuous function and $\phi(0) = 0$. However, since

$$\tan\phi(q) = -\frac{\pi^{\frac{3}{2}} q}{\mathcal{Z}_{00}(1, q^2)}$$

We then can plot $\phi(q)$ as

$$\phi(q) = \arctan\left(-\frac{\pi^{\frac{3}{2}} q}{\mathcal{Z}_{00}(1, q^2)}\right) \tag{2.7.1}$$

since the codomain of arctan is between $\pm\frac{\pi}{2}$, we would have a discontinuous $\phi(q)$ as

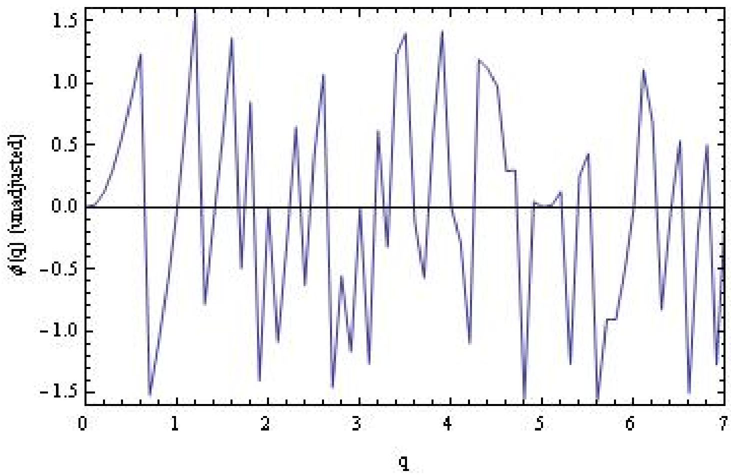

Fig. 2.7.1

In order to make $\phi(q)$ continuous, starting from $q = 0$ in the direction of increasing q, we should add appropriate multiples of π to $\phi(q)$ every time when $-\dfrac{\pi^{\frac{3}{2}} q}{\mathcal{Z}_{00}(1, q^2)}$ goes from ∞ to $-\infty$. The adjusted $\phi(q)$ is continuous

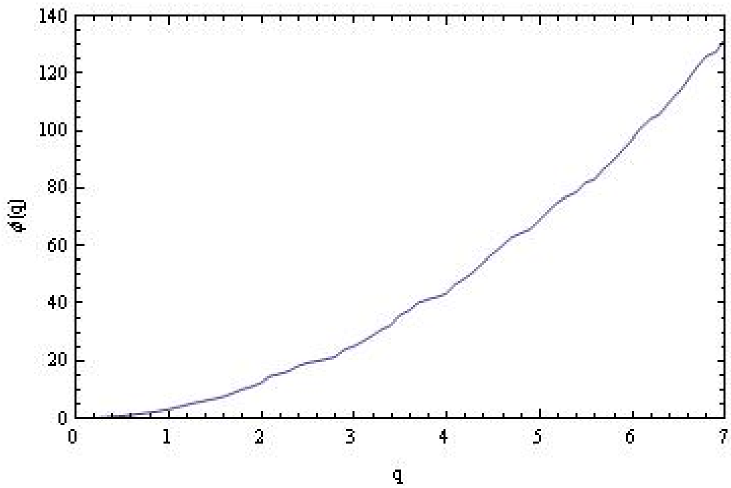

Fig. 2.7.2

and the adjustment does not affect the value of $e^{-2i\phi(q)}$ in Lüscher's formula. Since $k = \dfrac{2\pi}{L} q$, we can plot $\phi(q)$ and $r\pi - \delta_0(k)$ in the same diagram as in Fig. 2.7.4.

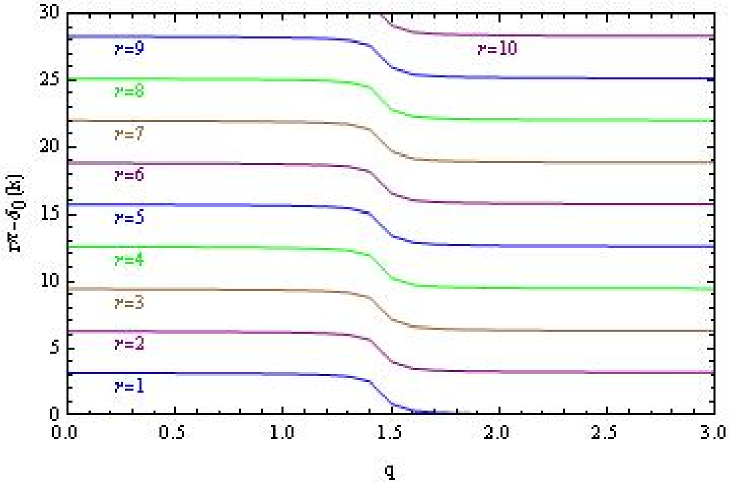

Fig. 2.7.3 $r\pi - \delta_0(k)$ at $L = 24$ $(1/m_\pi)$

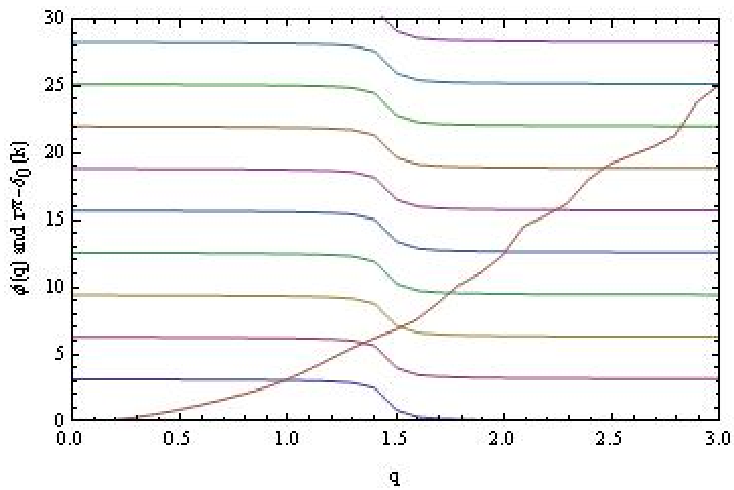

Fig. 2.7.4 Solutions of $\phi(q) = r\pi - \delta_0(k)$ at $L = 24$ $(1/m_\pi)$

In Fig. 2.7.4, the intersections where $\phi(q)$ crosses $r\pi - \delta_0(k)$ are solutions of

$$\phi(q) = r\pi - \delta_0(k), r \in \mathbb{N}$$

and at a fixed L we have a set of solutions. By identifying $\delta(k)$ in section 2.6 as $\delta_0(k)$, we can relate q and hence, k, in the finite volume scattering with the infinite volume phase shifts. And by

$$E = 2m_\pi + \frac{k^2}{2\mu}$$

$$k = 2\mu\sqrt{E - 2m_\pi}$$

$$q = \frac{L}{2\pi}2\mu\sqrt{E - 2m_\pi}$$

we have

$$\phi(\frac{L}{2\pi}2\mu\sqrt{E - 2m_\pi}) = r\pi - \delta(2\mu\sqrt{E - 2m_\pi})$$

Thus we can relate the energy spectrum of the finite volume scattering with the infinite volume phase shifts.

Chapter 3

Pion-Pion Scattering by Hypothetical Sigma

3.1 Overview

In this chapter we will study our model for $\sigma \to \pi\pi$ scattering problem in more detail.

Consider two-pion scattering with σ as the intermediate state in the low energy region above threshold. Our model is a non-relativistic one. We model the scattering in a finite volume lattice with settings as mentioned in Section 2.2 and 2.3. With the Hamiltonian operator acting on the wave function in the Schrödinger Equation

$$H\Psi = E\Psi$$

we can get the energy eigenvalues of the Hamiltonian, i.e. the energy spectrum of the finite volume scattering. By calculating the r matrix for $\pi\pi$ scattering, we can determine the infinite volume phase shifts, $\delta(k)$. With Lüscher's formula

$$e^{2i\delta_0(k)} = \frac{m_{00} + i}{m_{00} - i} = e^{-2i\phi(q)}$$

we can obtain the phase shifts in terms of the energy eigenvalues in finite volume scattering. Hence, we can study $\pi\pi$ scattering with our finite volume model, extracting, for example, the energy of the $\pi\pi$ resonance in the continuum.

3.2 Interaction Coupling

In the Hamiltonian matrix:

$$H = \begin{pmatrix} m_{\sigma 0} & \sqrt{C_0}g(k_0) & \sqrt{C_1}g(k_1) & \sqrt{C_2}g(k_2) & \cdots \\ \sqrt{C_0}g(k_0) & 2m_\pi & & & \\ \sqrt{C_1}g(k_1) & & 2m_\pi + \frac{k_1^2}{m_\pi} & & \\ \sqrt{C_2}g(k_2) & & & 2m_\pi + \frac{k_2^2}{m_\pi} & \\ \vdots & & & & \ddots \end{pmatrix}$$

there are non-zero off-diagonal terms $g(k)$. These involve the coupling constant, together with some momentum dependence:

$$g(k) = g(0)u(k)$$

where $u(k)$ is a form factor. $u(k)$ turns off the interaction in the high energy region while retaining the interaction in the low energy region. We set $g(0) = 0.13$ $(m_\pi^{-1/2})$ and adopt a form factor of Gaussian form

$$u(k) = e^{-\frac{k^2}{\Lambda^2}}$$

In our toy model, we set $m_\sigma = 2.1$ (m_π), choose

$$\Lambda \sim \sqrt{m_\pi m_\sigma}$$

and set $\Lambda = \sqrt{2.1}$ (m_π). Hence we have

$$g(k) = g(0)e^{-\frac{k^2}{\Lambda^2}}$$

with above mentioned $g(0)$ and Λ. The shape of the form factor $g(k)$ is shown in Fig. 3.2.1.

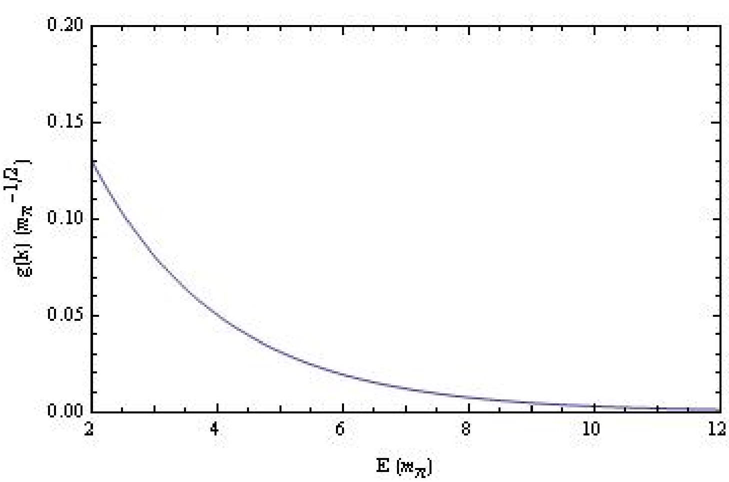

Fig. 3.2.1 Dependence of the form factor $g(k)$ on energy

For the discretized case such as $g(k_n)$ in the Hamiltonian, there should also be a factor $(\frac{2\pi}{L})^{\frac{3}{2}}$ because of the normalization. Hence

$$g(k_n) = (\frac{2\pi}{L})^{\frac{3}{2}} g(0) e^{-\frac{k_n^2}{\Lambda^2}}$$

and the Hamiltonian becomes

$$H = \begin{pmatrix} m_{\sigma 0} & \sqrt{C_0}(\frac{2\pi}{L})^{\frac{3}{2}} g(0) & \sqrt{C_1}(\frac{2\pi}{L})^{\frac{3}{2}} g(0) e^{-\frac{k_1^2}{\Lambda^2}} & \sqrt{C_2}(\frac{2\pi}{L})^{\frac{3}{2}} g(0) e^{-\frac{k_2^2}{\Lambda^2}} & \cdots \\ \sqrt{C_0}(\frac{2\pi}{L})^{\frac{3}{2}} g(0) & 2m_\pi & & & \\ \sqrt{C_1}(\frac{2\pi}{L})^{\frac{3}{2}} g(0) e^{-\frac{k_1^2}{\Lambda^2}} & & 2m_\pi + \frac{k_1^2}{m_\pi} & & \\ \sqrt{C_2}(\frac{2\pi}{L})^{\frac{3}{2}} g(0) e^{-\frac{k_2^2}{\Lambda^2}} & & & 2m_\pi + \frac{k_2^2}{m_\pi} & \\ \vdots & & & & \ddots \end{pmatrix}$$

3.3 Momentum Cutoff in the Hamiltonian

In the Hamiltonian describing the $\sigma \to \pi\pi$ interaction, although we have figured out the form of the elements, we have not figured out the dimension of the matrix. We have to give a finite dimension to our Hamiltonian, since numerically it is impossible to get the energy eigenvalues of a Hamiltonian of infinite volume. We should set a reasonable cutoff which would not greatly influence the energy eigenvalues.

First we note that, for an $m \times m$ matrix A_m, if $\{\lambda_1, \lambda_2 ... \lambda_m\}$ are its eigenvalues, then the $n \times n$ matrix A_n

$$A_n = \begin{pmatrix} \begin{pmatrix} & A_m & \end{pmatrix} & & & 0 & \\ & \lambda_{m+1} & & & \\ & & \lambda_{m+2} & & \\ 0 & & & \ddots & \\ & & & & \lambda_n \end{pmatrix}$$

has eigenvalues $\{\lambda_1, \lambda_2 ... \lambda_m, \lambda_{m+1}, \lambda_{m+2} ... \lambda_n\}$.

In our Hamiltonian, the off-diagonal elements are in the form $\sqrt{C_n}(\frac{2\pi}{L})^{\frac{3}{2}} g(0) e^{-\frac{k_n^2}{\Lambda^2}}$, which has a form factor $e^{-\frac{k_n^2}{\Lambda^2}}$. When k_n is very large, $e^{-\frac{k_n^2}{\Lambda^2}}$ will become very small, hence we have $\sqrt{C_n}(\frac{2\pi}{L})^{\frac{3}{2}} g(0) e^{-\frac{k_n^2}{\Lambda^2}} \sim 0$ for large k_n.

Hence, the infinite dimensional Hamiltonian $\tilde{H}$ can be approximated as

$$\tilde{H} = \begin{pmatrix} \begin{pmatrix} & & \\ & H & \\ & & \end{pmatrix} & \sim 0 & \sim 0 & \cdots \\ \sim 0 & \lambda_{m+1} & & \\ \sim 0 & & \lambda_{m+2} & \\ \vdots & & & \ddots \end{pmatrix}$$

where H is an $m \times m$ Hamiltonian with momentum cutoff. If H has eigenvalues $\{\lambda_1, \lambda_2 ... \lambda_m\}$, the eigenvalues of $\tilde{H}$ will approximately be the eigenvalues of H and non-interactive energy levels $\{\lambda_{m+1}, \lambda_{m+2} ...\}$, since the corresponding off-diagonal terms are close to 0. Hence, we can remove the rows and columns corresponding to very large momenta without influencing the remaining energy eigenvalues greatly. That is, we can impose a cutoff on the Hamiltonian.

We plot matrix dimensions and the lowest five energy eigenvalues with real momenta i.e. $W > 2m_\pi$ for different values of momentum cutoff, $k_{\max}$, for the Hamiltonian at different L's, as shown in Figs. 3.3.1 to 3.3.6.

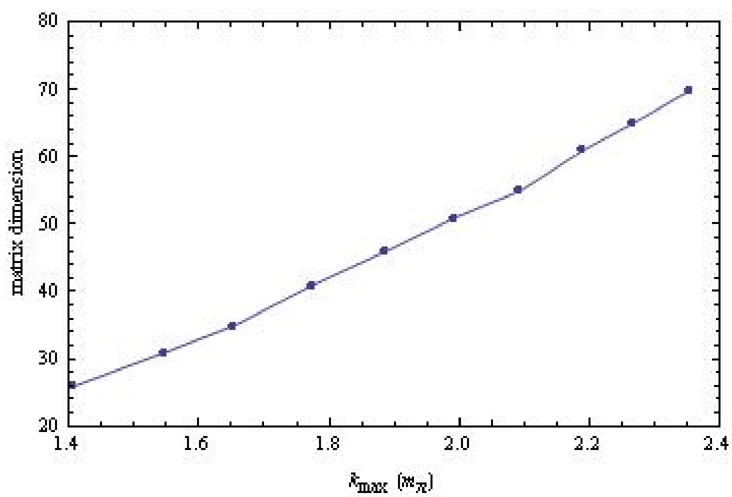

Fig. 3.3.1 Matrix dimensions at different $k_{\max}$ and at $L = 24$ $(1/m_\pi)$

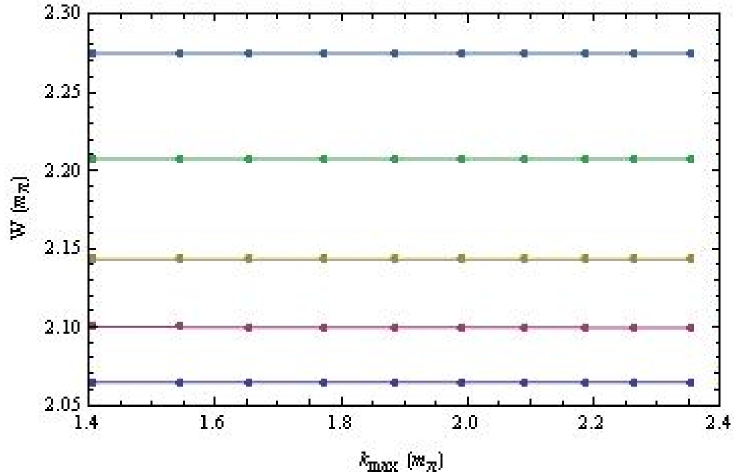

Fig. 3.3.2 Lowest five eigenvalues with real momenta at different $k_{\max}$ and at $L = 24$ $(1/m_\pi)$

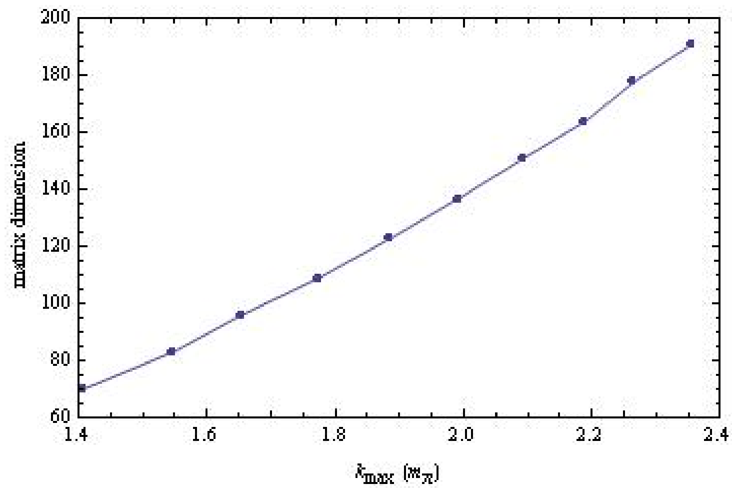

Fig. 3.3.3 Matrix dimensions at different $k_{\max}$ and at $L = 40$ $(1/m_\pi)$

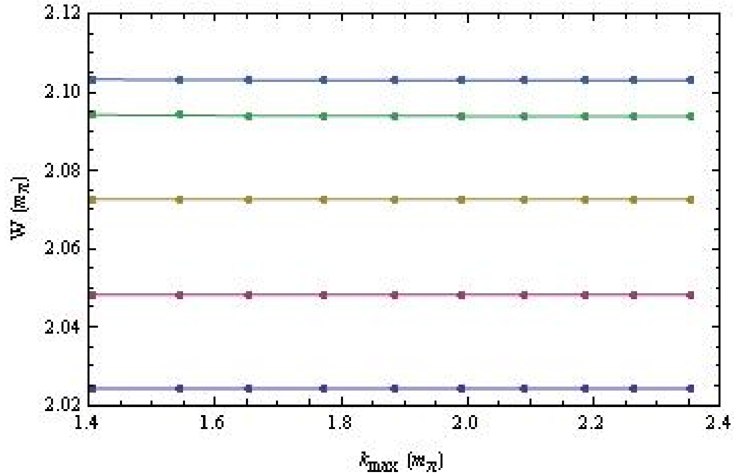

Fig. 3.3.4 Lowest five eigenvalues with real momenta at different $k_{\max}$ and at $L = 40$ $(1/m_\pi)$

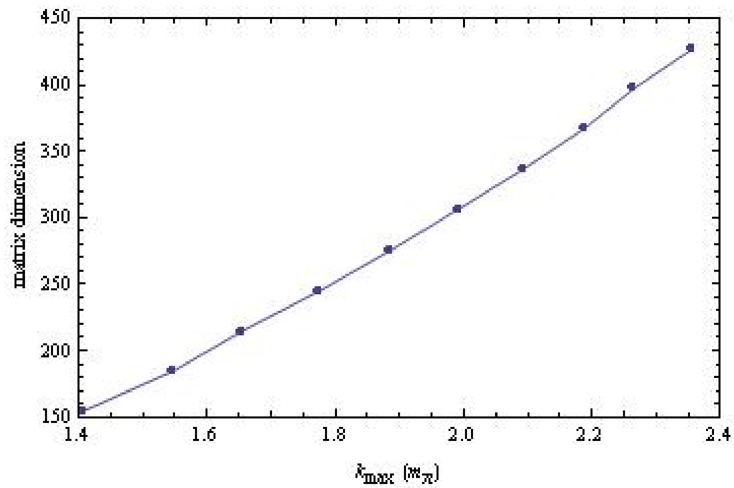

Fig. 3.3.5 Matrix dimensions at different $k_{\max}$ and at $L = 60$ $(1/m_\pi)$

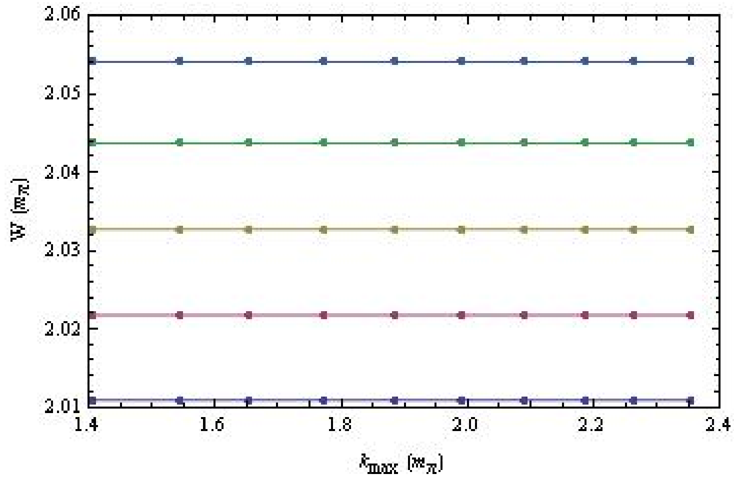

Fig. 3.3.6 Lowest five eigenvalues with real momenta at different $k_{\max}$ and at $L = 60$ $(1/m_\pi)$

We find that the lowest five eigenvalues do not change significantly according to different $k_{\max}$ in the plotted region. So the momentum is large enough in the plotted region to be chosen as the momentum cutoff $k_{\max}$ for the Hamiltonian. We choose $k_{\max} \sim 4.4\ m_\pi$ in our model.

3.4 Energy Spectrum

By working on a finite volume lattice, we will get a discrete energy spectrum from the eigenvalues of the Hamiltonian operator for the scattering process, as shown in Fig. 3.4.1.

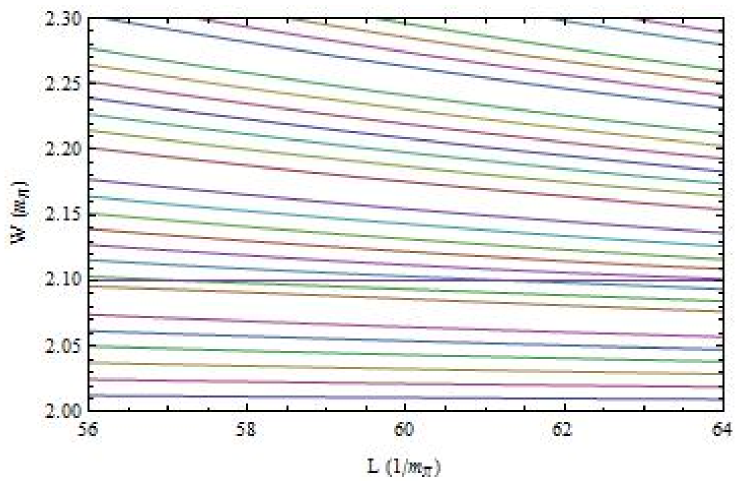

Fig. 3.4.1 Energy Spectrum of the $\sigma \to \pi\pi$ system around $L = 60$ $(1/m_\pi)$ with m_σ marked as the horizontal line at $W = 2.1$ (m_π)

Each line of the energy spectrum corresponds to the energy of an eigenstate of the Hamiltonian operator. However, Ψ is not an energy eigenstate of the Hamiltonian operator in infinite volume but a mixture of the energy eigenstates.

At a fixed lattice size, we can get a set of energy eigenvalues, as shown in Fig. 3.4.2.

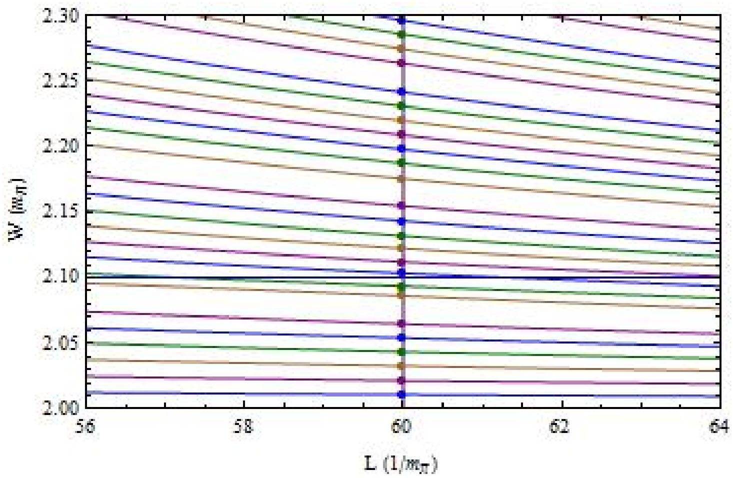

Fig. 3.4.2 Energy eigenvalues (dots) of $\sigma \to \pi\pi$ scattering at $L = 60$ $(1/m_\pi)$ with m_σ marked as the horizontal line at $W = 2.1$ (m_π)

Since Ψ is a mixture of the eigenstates of the Hamiltonian operator, none of the energy eigenvalues in Fig. 3.4.2 corresponds to the exact resonance energy, or the exact resonance mass. However, we can extract the phase shifts of these energy eigenvalues by Lüscher's formula and try to locate the mass of the resonance.

3.5 Quasi-Infinite Volume Phase Shifts

By imposing finite volume conditions, we have acquired a discrete energy spectrum. We can also find the influence of finite volume conditions on the r-matrix. From (2.6.9), in the infinite volume case, the r-matrix is

$$\frac{g^2(k)}{\frac{k_0^2}{2\mu} + 2m_\pi - m_{\sigma 0} - 2\mu P \int_0^\infty \frac{dk' k'^2 g^2(k')}{k_0^2 - k'^2 + i\eta}} = r_l(k, k; \frac{k_0^2}{2\mu}) = -\frac{\tan \delta_l}{\pi \mu k_0}$$

From

$$P \int_0^\infty \frac{f(x)}{x^2 - a^2} dx = \int_0^\infty \frac{f(x) - f(a)}{x^2 - a^2} dx$$

and since for spherically symmetric function $f(x)$

$$\int_0^\infty dx x^2 f(x) = \frac{1}{4\pi}\int d\Omega \int_0^\infty dx x^2 f(x) = \frac{1}{4\pi}\int d^3x f(x)$$

we have

$$\begin{aligned} P\int_0^\infty \frac{dk'k'^2g^2(k')}{k^2-k'^2+i\eta} &= -P\int_0^\infty \frac{dk'k'^2g^2(k')}{k'^2-k^2-i\eta} \\ &= -\int_0^\infty dk' \frac{k'^2g^2(k')-k^2g^2(k)}{k'^2-k^2} \\ &= -\int_0^\infty dk' \frac{k'^2g^2(k')}{k'^2-k^2} + \int_0^\infty dk' \frac{k^2g^2(k)}{k'^2-k^2} \\ &= -\int_0^\infty dk' \frac{k'^2g^2(k')}{k'^2-k^2} + \int_0^\infty dk' \frac{k'^2k^2g^2(k)}{k'^2(k'^2-k^2)} \\ &= -\frac{1}{4\pi}\int_0^\infty d^3k' \frac{g^2(k')}{k'^2-k^2} + \frac{1}{4\pi}\int_0^\infty d^3k' \frac{k^2g^2(k)}{k'^2(k'^2-k^2)} \end{aligned}$$

In finite volume case, we can discretize the integral with the following substitutions:

$$\int d^3k' f(k') \to \sum_q (\frac{2\pi}{L})^3 C_q f(k_q)$$

with C_q the number of distinct 3-D vectors $\mathbf{n} = (n_1, n_2, n_3)$ where $n_1, n_2, n_3, |\mathbf{n}| \in \mathbb{Z}$ and $|\mathbf{n}| = q$. Then by putting

$$g(k) = g(0)e^{-\frac{k^2}{\Lambda^2}}$$

and through discretized version of (2.6.9) we have

$$\frac{g^2(k)}{\frac{k^2}{2\mu} + 2m_\pi - m_{\sigma 0} - 2\mu\Sigma} = -\frac{\tan\delta}{\pi\mu k}$$

where

$$\Sigma = -\frac{1}{4\pi}(\frac{2\pi}{L})^3 \sum_{q=1}^{\infty} \frac{C_q(g_0 e^{-\frac{(\frac{2\pi}{L})^2 m}{\Lambda^2}})^2}{(\frac{2\pi}{L})^2 q - 2\mu(W-2m_\pi)} + \frac{1}{4\pi}(\frac{2\pi}{L})^3 \sum_{q=1}^{\infty} \frac{C_q 2\mu(W-2m_\pi)(g_0 e^{-\frac{2\mu(W-2m_\pi)}{\Lambda^2}})^2}{(\frac{2\pi}{L})^2 q((\frac{2\pi}{L})^2 q - 2\mu(W-2m_\pi))}$$

So we have

$$\delta = \arctan(\frac{-\pi\mu k g^2(k)}{\frac{k^2}{2\mu} + 2m_\pi - m_{\sigma 0} - 2\mu\Sigma})$$

Of course, the δ here is not the phase shift of the real infinite volume case. Hence, we shall call the such δ calculated from the discretized r-matrix with finite volume conditions "quasi phase shift".

In numerical calculation, we have to give q an upper limit to the discrete sum over q. Since we have a term $e^{-\frac{(\frac{2\pi}{L})^2 q^2}{\Lambda^2}}$ within the sum, we set the upper limit at $10L$.

We can observe the influence of finite volume conditions by plotting the quasi infinite volume phase shifts against different L's.

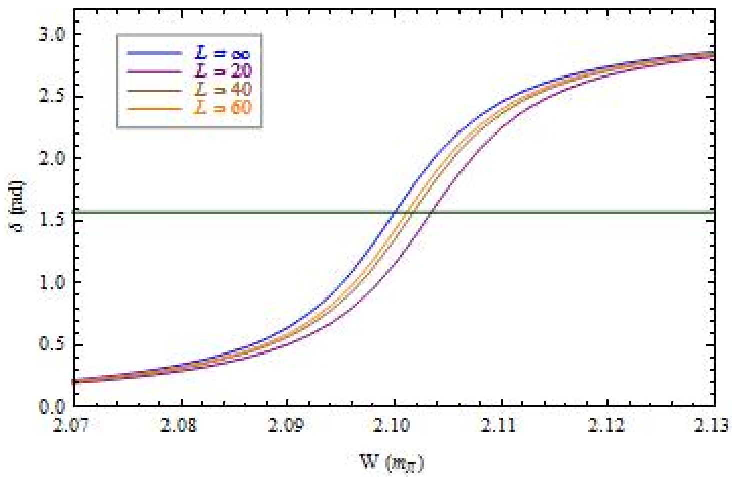

Fig. 3.5.1 Infinite Volume Phase Shifts ($L = \infty$) and Quasi Phase Shifts at different L's with L in the unit of $1/m_\pi$

As shown in Fig. 3.5.1, the curves of the quasi infinite volume phase shifts move towards to the curve of the real infinite volume phase shifts. This is in agreement with the expectation, as the model approaches infinite volume scattering.

3.6 Extracting Phase Shifts from the Energy Spectrum

For an infinite volume scattering process, the allowed phase shifts of the resonance form a continuous curve, with Fig. 2.6.1 as an example. When the energy is at the resonance mass, the phase shift is $\frac{\pi}{2}$.

For a finite volume scattering process, the allowed energies of the system take a series of discrete values. By Lüscher's formalism, they correspond to the solutions, with Fig. 2.7.4 as an example. Hence, by applying Lüscher's formula to the energy eigenvalues of the Hamiltonian established in Section 3.2 and 3.3, we can acquire the corresponding phase shifts.

For the finite volume case, the allowed k's are

$$k = \frac{2\pi}{L} |\mathbf{n}| , \mathbf{n} \in \mathbb{Z}^3$$

Hence, we will have a discrete sum over k's. From 2.7.1

$$\phi(q) = \arctan(-\frac{\pi^{\frac{3}{2}} q}{\mathcal{Z}_{00}(1, q^2)})$$

where

$$\mathcal{Z}_{00}(1, q^2) = \frac{1}{\sqrt{4\pi}}(-\frac{1}{q^2} + J_0 + J_1 q^2 + \sum_{N=1}^{\infty} C_N \frac{q^4}{N^2(N - q^2)})$$

as in Section 2.5. Hence we have

$$\delta = \arctan(\frac{\pi^{\frac{3}{2}} q}{\frac{1}{\sqrt{4\pi}}(-\frac{1}{q^2} + \sum\limits_{m=1}^{\infty}(\frac{q^4}{m^2(m-q^2)} + \frac{q^2}{m^2}))})$$

Then, for the x-th lowest energy eigenvalue W_x, we have

$$\delta_x = \arctan(\frac{\pi^{\frac{3}{2}} q_x}{\frac{1}{\sqrt{4\pi}}(-\frac{1}{q_x^2} + \sum\limits_{m=1}^{\infty}(\frac{q_x^4}{m^2(m-q_x^2)} + \frac{q_x^2}{m^2}))})$$

Replacing q_x by $(\frac{L}{2\pi})\sqrt{2\mu(W_x - 2m_\pi)}$, we have

$$\delta_x = \arctan(\frac{\pi^{\frac{3}{2}}(\frac{L}{2\pi})\sqrt{2\mu(W_x - 2m_\pi)}}{\frac{1}{\sqrt{4\pi}}(-\frac{1}{(\frac{L}{2\pi})^2(2\mu(W_x-2m_\pi))} + \sum\limits_{m=1}^{\infty}(\frac{(\frac{L}{2\pi})^4(2\mu(W_x-2m_\pi))^2}{m^2(m-(\frac{L}{2\pi})^2(2\mu(W_x-2m_\pi)))} + \frac{(\frac{L}{2\pi})^2(2\mu(W_x-2m_\pi))}{m^2}))}) \tag{3.6.1}$$

By (3.6.1), we can extract the phase shift of a specific energy eigenvalue through Lüscher's formalism.

In numerical calculation, we need an upper limit for the m in (3.6.1). We make this upper limit adaptively increasable. In the codes, we compare the sum for $m = 1$ to n, denoted by S, and the sum for $m = n+1$ to $n+1000$, denoted by S_n. When $\dfrac{S_n}{S}$ is smaller than a certain acceptable value, then the loop is stopped, the upper limit is $m = n + 1000$, and $S + S_n$ is assigned to the sum. If not, then we increase m by 1000 and repeat the process.

In the following plots, shown in Figs. 3.6.1 through 3.6.10, the phase shifts acquired by Lüscher's formula at different values of L.

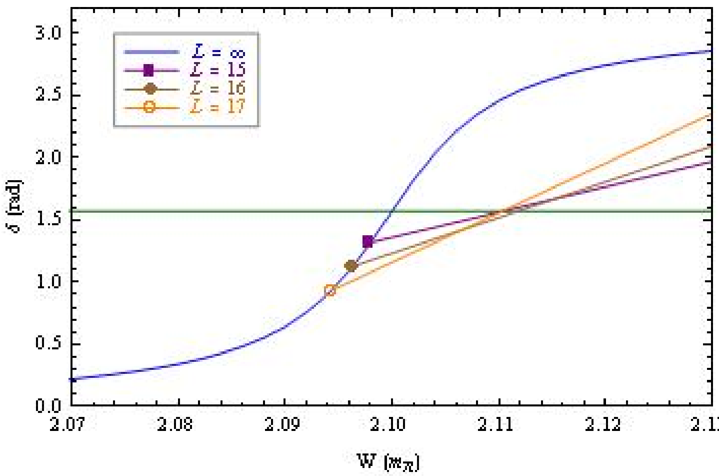

Fig. 3.6.1 Infinite volume phase shifts ($L = \infty$) and phase shifts at $L = 15$, 16, and 17 (m_π).

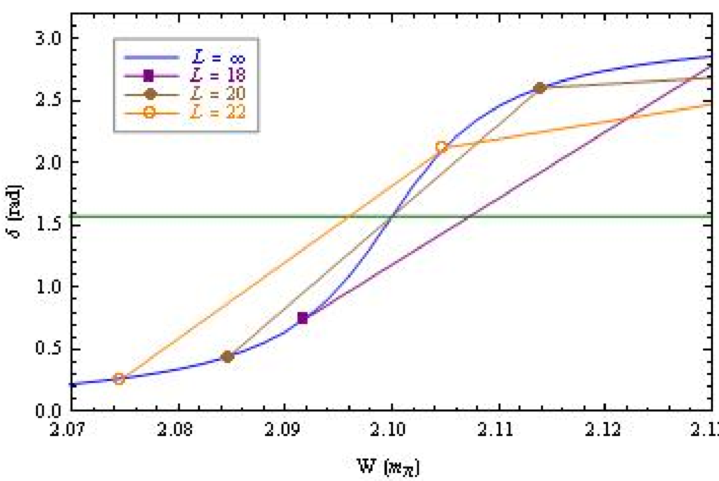

Fig. 3.6.2 Infinite volume phase shifts ($L = \infty$) and phase shifts at $L = 18$, 20, and 22 (m_π).

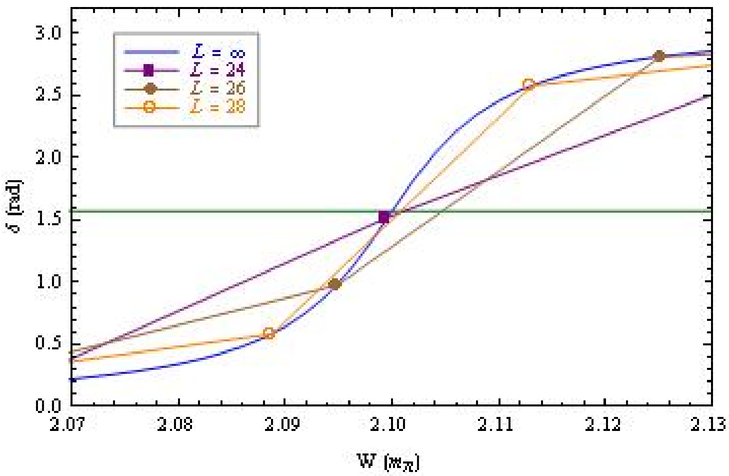

Fig. 3.6.3 Infinite volume phase shifts ($L = \infty$) and phase shifts at $L = 24$, 26, and 28 (m_π).

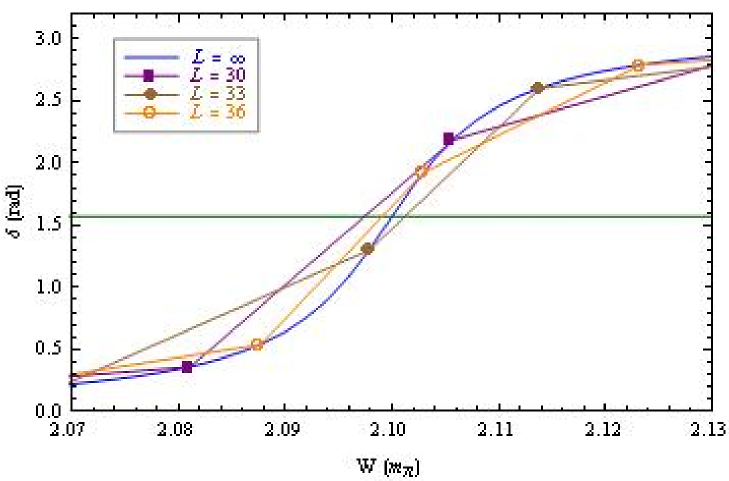

Fig. 3.6.4 Infinite volume phase shifts ($L = \infty$) and phase shifts at $L = 30$, 33, and 36 (m_π).

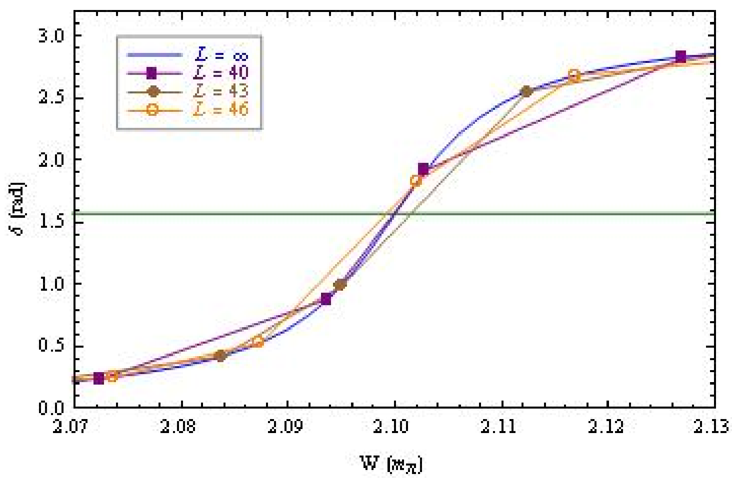

Fig. 3.6.5 Infinite volume phase shifts ($L = \infty$) and phase shifts at $L = 40$, 43, and 46 (m_π).

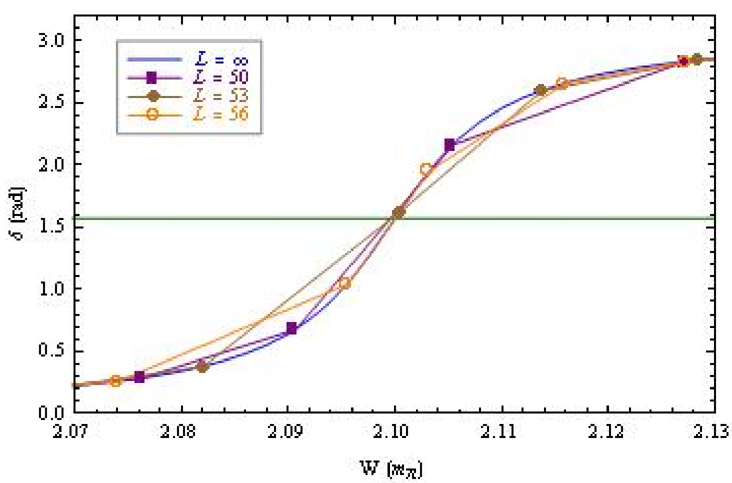

Fig. 3.6.6 Infinite volume phase shifts ($L = \infty$) and phase shifts at $L = 50$, 53, and 56 (m_π).

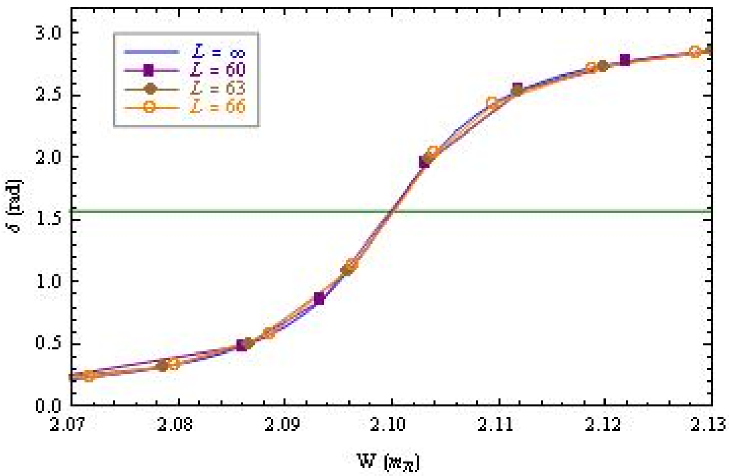

Fig. 3.6.7 Infinite volume phase shifts ($L = \infty$) and phase shifts at $L = 60$, 63, and 66 (m_π).

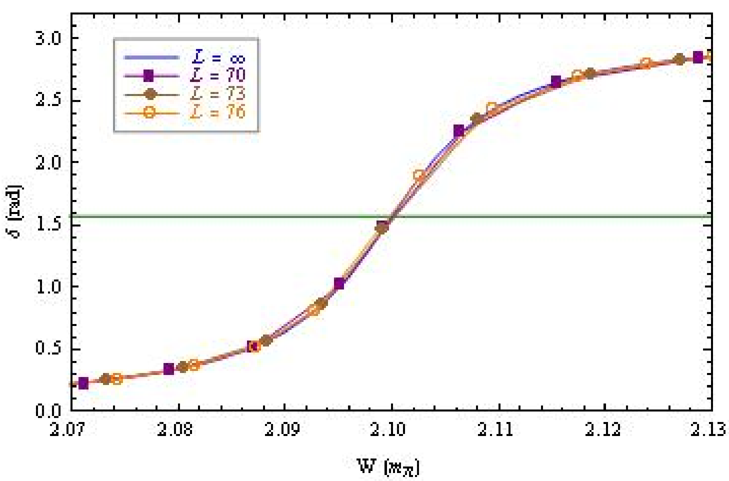

Fig. 3.6.8 Infinite volume phase shifts ($L = \infty$) and phase shifts at $L = 70$, 73, and 76 (m_π).

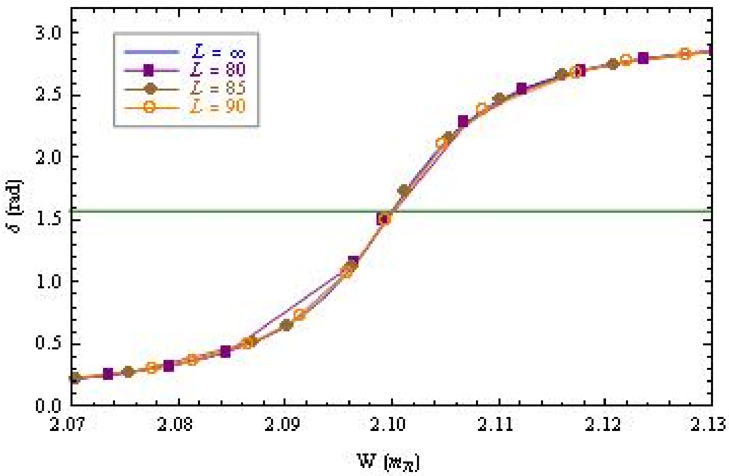

Fig. 3.6.9 Infinite volume phase shifts ($L = \infty$) and phase shifts at $L = 80$, 85, and 90 (m_π).

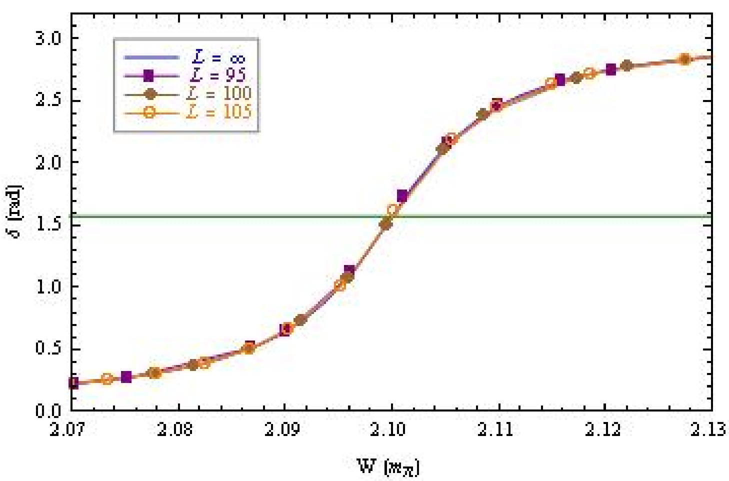

Fig. 3.6.10 Infinite volume phase shifts ($L = \infty$) and phase shifts at $L = 95$, 100, and 105 (m_π).

We can observe that the phase shifts extracted from Lüscher's formula approach the infinite volume phase shifts as the lattice size increases.

In Fig. 3.6.1 to Fig. 3.6.10, the finite volume phase shifts calculated from Lüscher's method are discrete dots and do not fall exactly on the pole position. We calculated the pole position by interpolation, which coresponds to the intersection of the straight line between the two closest dot below and above the pole and the horizontal line which marks $\delta = \dfrac{\pi}{2}$. In Fig. 3.6.1 to Fig. 3.6.10, all of the dots representing phase shifts extracted from Lüscher's formula lie very close to the curve of the exact infinite volume phase shift. This means that Lüscher's formula works quite well at $L > 15\ 1/m_\pi$. By observing cases with smaller values of L, for example, in Fig. 3.6.1 and Fig. 3.6.2, we can find that the problem of deciding the pole position comes from the scarce numbers of dots of phase shifts extracted from Lüscher's formula, which caused the deviations of the pole position calculated by interpolation. In cases of larger values of L, for example, in Fig. 3.6.9 and Fig. 3.6.10, with more densely distributed dots of phase shifts extracted from Lüscher's formula, the deviations of the pole position calculated by interpolation decrease significantly.

Another factor which may cause the deviations of the pole position is the finite volume effect. The finite volume effect is exponentially suppressed as the lattice size increases. As L approaches ∞, the finite volume phase shifts approach to the exact infinite volume phase shift.

We use a linear fit to obtain the finite volume phase shifts at the pole position and denote it δ_L, where L is the side length of the lattice. At the pole position, the infinite volume phase shift, δ_∞, is $\dfrac{\pi}{2}$. We calculate the difference ratio $\dfrac{\delta_L - \delta_\infty}{\delta_L}$ for the $\sigma \to \pi\pi$ scattering. The difference ratio $\dfrac{\delta_L - \delta_\infty}{\delta_L}$ is plotted against L as shown in Fig. 3.6.11.

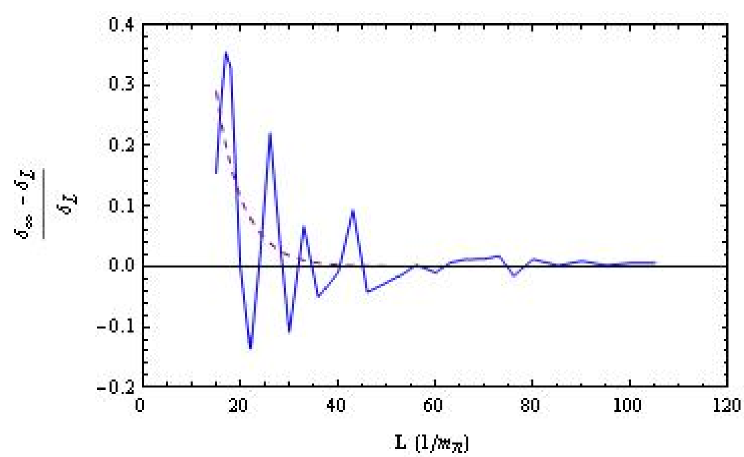

Fig. 3.6.11 Difference ratio between finite and infinite volume phase shifts (solid line) and its exponential fit (dashed line) of the $\sigma \to \pi\pi$ scattering

In Fig. 3.6.11, we can find that at smaller L values, the oscillation of the difference ratio $\dfrac{\delta_L - \delta_\infty}{\delta_L}$ is larger. The larger oscillation at smaller L values is because of the scarce numbers of dots of phase shifts extracted from Lüscher's method. Hence, the pole positions calculated by interpolating these dots are prone to be influenced by the positions of neighboring dots calculated by Lüscher's method from the energy eigenvalues.

We use an exponential fit to plot the relation between the difference ratio $\dfrac{\delta_L - \delta_\infty}{\delta_L}$ and L, which is shown as the dashed line in Fig. 3.6.11. We can find that, besides the oscillation mentioned above, the absolute value of the difference ratio in exponential fit diminishes as L increases. This result is in accordance with the decrease of finite volume effect at larger values of L as expected.

Chapter 4

Rho-Pion Scattering

4.1 Overview

In this chapter we apply our toy model to a vector meson in the real world. We will investigate the π-π scattering in $\rho \to \pi\pi$ channel first and then with both $\rho \to \pi\pi$ and $\rho \to \pi\omega$ channels included.

The ρ meson is a vector meson with total spin 1 and odd parity. The ω meson is also a vector meson with total spin 1 and odd parity, while the π is a pseudoscalar meson with total spin 0 and odd parity. The self-energy of the ρ meson through the $\rho \to \pi\pi$ channel is shown in Fig. 4.1.1.

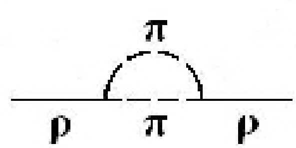

Fig. 4.1.1

The decay of the ρ meson in $\rho \to \pi\omega$ channel is shown in Fig. 4.1.2.

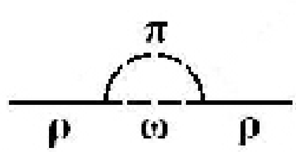

Fig. 4.1.2

We will attend to the scattering phase shifts first and then to the finite volume estimates of the phase shifts.

4.2 R-matrix for Pi-Pi Scattering in Rho Decay

In this section we only consider the $\rho \to \pi\pi$ channel. The pole is situated at about 5 to 6 m_π, so instead of treating the energy non-relativistically as in Chapter 3, we adopt a relativistic picture. For the decay of the ρ meson in the $\rho \to \pi\pi$ channel in Fig. 4.1.1, the t-matrix takes the form

$$t(k,k,E^+) = \frac{G^2(k)}{E^2 - m_\rho^2} = \frac{G^2(k)}{E^2 - m_{\rho 0}^2 - \Sigma_{\rho\pi\pi}(E^+)} = A(k)e^{i\delta(k)}\sin\delta(k)$$

where

$$E = 2\omega_k = 2\sqrt{k_E^2 + m_\pi^2}$$

$G(k)$ is a coupling parameter, $\Sigma_{\rho\pi\pi}(E^+)$ is the ρ meson self energy correction term, and $A(k)$ is a normalized factor associated with the pole in the self energy denominator.

From[23]

$$\begin{aligned}
\Sigma_{\rho\pi\pi}(E^+) &= -\frac{f_{\rho\pi\pi}^2}{3\pi^3}\int d^3k' \frac{k'^2 u^2(k')}{(2\omega_{k'})((2\omega_{k'})^2 - E^2 - i\eta)} \\
&= \frac{f_{\rho\pi\pi}^2}{3\pi^3}\int d^3k' \frac{k'^2 u^2(k')}{(2\omega_{k'})(E^2 - (2\omega_{k'})^2 + i\eta)} \\
&= \frac{2f_{\rho\pi\pi}^2}{3\pi^2}\int dk' \frac{k'^4 u^2(k')}{\omega_{k'}(E^2 - (2\omega_{k'})^2 + i\eta)}
\end{aligned}$$

and from

$$\Sigma_{\rho\pi\pi}(E^+) = \int dk' \frac{k'^2 G^2(k')}{E^2 - (2\omega_{k'})^2 + i\eta}$$

by comparison we have

$$G^2(k) = \frac{2f_{\rho\pi\pi}^2}{3\pi^2}\frac{k^2 u^2(k)}{\omega_k}$$

where $u(k)$ is a form factor. We define the resonance position as the point at which the real part of the full ρ-propagator passes through zero,

$$E^2 - m_{\rho 0}^2 - \Sigma_{\rho\pi\pi}(m_\rho) = 0$$

$$m_\rho^2 = m_{\rho 0}^2 + \Sigma_{\rho\pi\pi}(m_\rho)$$

hence

$$t_{pole} = \frac{G^2_{pole}(k)}{E^2 - m^2_{\rho 0} - \Sigma_{\rho\pi\pi}(m_\rho)} = -\frac{G^2_{pole}(k)}{\operatorname{Im}\Sigma_{\rho\pi\pi}(m_\rho)}$$

At the pole we also have

$$\delta = \frac{\pi}{2}$$

so

$$t_{pole} = A(k_{pole}) \cdot i$$

Let

$$k_{pole} = p = \sqrt{\frac{m^2_\rho}{4} - m^2_\pi}$$

then

$$t_{pole} = A(p) \cdot i$$

Since the energy at the pole has the following form

$$m^2_\rho = 4(p^2 + m^2_\pi)$$

then the imaginary part of $\Sigma_{\rho\pi\pi}$ has the form

$$\begin{aligned} -\operatorname{Im}\Sigma_{\rho\pi\pi}(m_\rho) &= -\operatorname{Im}(\frac{2f^2_{\rho\pi\pi}}{3\pi^2}\int_0^\infty dk' \frac{k'^4 u^2(k)}{\omega_{k'}(m^2_\rho - (2\omega_{k'})^2 + i\eta)}) \\ &= -\operatorname{Im}(\frac{2f^2_{\rho\pi\pi}}{3\pi^2}\int_0^\infty dk' \frac{k'^4 u^2(k')}{\omega_{k'} \cdot 4(p^2 - k'^2 + i\eta)}) \\ &= \frac{f^2_{\rho\pi\pi}}{6\pi^2}\int_0^\infty dk' \frac{k'^4 u^2(k')}{\omega_{k'}} \cdot i\pi\delta(p^2 - k'^2) \end{aligned}$$

By using the relation for a Direc delta function

$$\delta(x^2 - a^2) = \frac{1}{|2a|}\delta(x - a)$$

we have

$$\begin{aligned} -\operatorname{Im}\Sigma_{\rho\pi\pi}(m_\rho) &= \frac{if^2_{\rho\pi\pi}}{6\pi}\int_0^\infty dk' \frac{k'^4 u^2(k')\delta(p - k')}{\omega_{k'}\,|2p|} \\ &= \frac{if^2_{\rho\pi\pi} p^3 u^2(p)}{12\pi\omega_p} \end{aligned}$$

then the t-matrix at the pole is

$$
\begin{aligned}
t_{pole} &= \frac{G_{pole}^2}{-\operatorname{Im}\Sigma_{\rho\pi\pi}} \\
&= \frac{\frac{2f_{\rho\pi\pi}^2}{3\pi^2}\frac{p^2u^2(p)}{\omega_p}}{\frac{if_{\rho\pi\pi}^2p^3u^2(p)}{12\pi\omega_p}} \\
&= -\frac{8i}{\pi p}
\end{aligned}
$$

and we can derive the normalized factor $A(k)$ from

$$
A(p) = -\frac{8}{\pi p}
$$

$$
\Longrightarrow A(k) = -\frac{8}{\pi k}
$$

So the relationship between the t-matrix $t(k)$ and the phase shift $\delta(k)$, in this case is

$$
t(k) = -\frac{8}{\pi k}e^{-i\delta(k)}\sin\delta(k)
$$

So we find

$$
\frac{G^2(k)}{E^2 - m_{\rho 0}^2 - \Sigma_{\rho\pi\pi}(E^+)} = t(k) = -\frac{8}{\pi k}e^{-i\delta(k)}\sin\delta(k) \tag{4.2.1}
$$

and the r-matrix is

$$
\frac{G^2(k)}{s - m_{\rho 0}^2 - P\Sigma_{\rho\pi\pi}(E)} = r(k) = -\frac{8}{\pi k}\tan\delta(k) \tag{4.2.2}
$$

The principal value of the loop integral $\Sigma_{\rho\pi\pi}$ is

$$
\begin{aligned}
P\Sigma_{\rho\pi\pi}(E) &= \frac{2f_{\rho\pi\pi}^2}{3\pi^2}P\int_0^\infty dk'\frac{k'^4u^2(k')}{\omega_{k'}(E^2-(2\omega_{k'})^2)} \\
&= -\frac{2f_{\rho\pi\pi}^2}{3\pi^2}P\int_0^\infty dk'\frac{k'^4u^2(k')}{\omega_{k'}((2\omega_{k'})^2-E^2)} \\
&= -\frac{2f_{\rho\pi\pi}^2}{3\pi^2}P\int_0^\infty dk'\frac{1}{4\omega_{k'}}\frac{k'^4u^2(k')}{k'^2-(\frac{1}{4}E^2-m_\pi^2)} \\
&= -\frac{f_{\rho\pi\pi}^2}{6\pi^2}P\int_0^\infty dk'\frac{1}{\omega_k'}\frac{k'^4u^2(k')}{k'^2-k^2}
\end{aligned}
$$

Since

$$
P\int_0^\infty dx\frac{1}{x^2-a^2} = 0
$$

$$
P\int_0^\infty dx\frac{f(a)}{x^2-a^2} = 0
$$

$$P\int_0^\infty dx \frac{f(x)}{x^2-a^2} = P\int_0^\infty dx \frac{f(x)-f(a)}{x^2-a^2}$$

When $f(x)$ has a factor of x, then $f(x)-f(a)$ has a factor of $x-a$, hence there left a factor $x+a$ in the denominator and the integral is real. In this case the principal integral becomes a standard integral:

$$P\int_0^\infty dx \frac{f(x)}{x^2-a^2} = \int_0^\infty dx \frac{f(x)-f(a)}{x^2-a^2}$$

So we can write

$$\begin{aligned} P\Sigma_{\rho\pi\pi}(E) &= -\frac{f^2_{\rho\pi\pi}}{6\pi^2}\int_0^\infty dk' \frac{1}{k'^2-k^2}\left(\frac{k'^4u^2(k')}{\omega_{k'}} - \frac{k^4u^2(k)}{\omega_k}\right) \\ &= -\frac{f^2_{\rho\pi\pi}}{6\pi^2}\int_0^\infty dk' \frac{1}{k'^2-k^2}\left(\frac{k'^4u^2(k')}{\sqrt{k'^2+m_\pi^2}} - \frac{k^4u^2(k)}{\sqrt{k^2+m_\pi^2}}\right) \end{aligned} \tag{4.2.3}$$

Substituting $P\Sigma_{\rho\pi\pi}(E)$ into (4.2.2) and using (4.2.3) we have

$$\frac{\frac{2f^2_{\rho\pi\pi}}{3\pi^2}\frac{k^2u^2(k)}{\omega_k}}{4(k^2+m_\pi)^2 - m^2_{\rho 0} + \frac{f^2_{\rho\pi\pi}}{6\pi^2}\int_0^\infty dk' \frac{1}{k'^2-k^2}\left(\frac{k'^4u^2(k')}{\sqrt{k'^2+m_\pi^2}} - \frac{k^4u^2(k)}{\sqrt{k^2+m_\pi^2}}\right)} = r(k) = -\frac{8}{\pi k}\tan\delta(k)$$

We can get the value of $m_{\rho 0}$ by fitting it so that the pole occurs at $E = 2\sqrt{k^2+m_\pi} = m_\rho$ and $\delta(k) = \frac{\pi}{2}$.

4.3 R-matrix for Infinite Volume Rho Decay with Linear Denominator

In the last section we found the r-matrix, as shown in (4.2.1). In order to match the propagator appearing in the Feynmann diagramms associated with $\rho \to \pi\pi$, the Green's function on left hand side of (4.2.1) has the form $\frac{1}{E^2-H^2}$ of which the denominator is quadratic. In order to simplify the solution of the problem using Hamiltonian methods on a finite lattice, we choose to linearize the problem. That is, we take the Green's function in the from $\frac{1}{E-H}$.

The t-matrix with a linear denominator takes the form

$$t(k,k,E^+) = \frac{G^2}{E - m_{\rho 0} - \frac{\Sigma_{\rho\pi\pi}(E^+)}{2m_{\rho 0}}} = A(k)e^{i\delta(k)}\sin\delta(k)$$

The normalization factor, $A(k)$, must be re-evaluated. At the pole, let

$$k_{pole} = p = \sqrt{\frac{m_\rho^2}{4} - m_\pi^2}$$

then we have

$$t_{pole} = \frac{G_{pole}^2}{m_\rho - m_{\rho 0} - \frac{\Sigma_{\rho\pi\pi}(m_\rho)}{2m_{\rho 0}}} = -\frac{2m_{\rho 0} G_{pole}^2}{\operatorname{Im}\Sigma_{\rho\pi\pi}(m_\rho)}$$

and

$$t_{pole} = A(p) \cdot i$$

So

$$\begin{aligned} t_{pole} &= 2m_{\rho 0} \frac{\frac{2f_{\rho\pi\pi}^2}{3\pi^2} \frac{p^2 u^2(p)}{\omega_p}}{\frac{i f_{\rho\pi\pi}^2 p^3 u^2(p)}{12\pi\omega_p}} \\ &= -\frac{16 m_{\rho 0} i}{\pi p} \\ A(p) &= -\frac{16 m_{\rho 0}}{\pi p} \\ \Longrightarrow A(k) &= -\frac{16 m_{\rho 0}}{\pi k} \end{aligned}$$

This is the form of the t-matrix with a linear denominator

$$\frac{G^2}{E - m_{\rho 0} - \frac{\Sigma_{\rho\pi\pi}(E^+)}{2m_{\rho 0}}} = t(k) = -\frac{16 m_{\rho 0}}{\pi k} e^{-i\delta(k)} \sin\delta(k) \tag{4.3.1}$$

and the r-matrix is

$$\frac{G^2(k)}{E - m_{\rho 0} - \frac{P\Sigma_{\rho\pi\pi}(E)}{2m_{\rho 0}}} = r(k) = -\frac{16 m_{\rho 0}}{\pi k} \tan\delta(k) \tag{4.3.2}$$

Substituting $P\Sigma_{\rho\pi\pi}(E)$ into (4.3.2) using (4.2.3), we have

$$\frac{\frac{2f_{\rho\pi\pi}^2}{3\pi^2} \frac{k^2 u^2(k)}{\omega_k}}{2\sqrt{(k^2 + m_\pi)^2} - m_{\rho 0} + \frac{1}{2m_{\rho 0}} \frac{f_{\rho\pi\pi}^2}{6\pi^2} \int_0^\infty dk' \frac{1}{k'^2 - k^2} \left(\frac{k'^4 u^2(k')}{\sqrt{k'^2 + m_\pi^2}} - \frac{k^4 u^2(k)}{\sqrt{k^2 + m_\pi^2}} \right)} = r(k) = -\frac{16 m_{\rho 0}}{\pi k} \tan\delta(k) \tag{4.3.3}$$

This is the r-matrix with a linear energy denominator which we want to find.

We can get the value of $m_{\rho 0}$ by fitting it so that the pole occurs at $E = 2\sqrt{k^2 + m_\pi} = m_\rho$ and $\delta(k) = \frac{\pi}{2}$.

The form factor $u(k)$ appearing in (4.3.3) is taken to be

$$u(k) = \frac{e^{-\frac{k^4}{\Lambda^4}}}{e^{-\frac{p^4}{\Lambda^4}}}$$

which is of a Gaussian-like form. The reason for the factor $e^{-\frac{p^4}{\Lambda^4}}$ in $u(k)$ is so that the $\rho \to \pi\pi$ coupling, which is matched to give the experimental value for the resonance width, is not scaled at the pole $k = p$.

The vertex function is

$$G(k) = \sqrt{\frac{2 f_{\rho\pi\pi}^2}{3\pi^2}} \frac{k u(k)}{\sqrt{\omega_k}}$$

which is shown in Fig. 4.3.1.

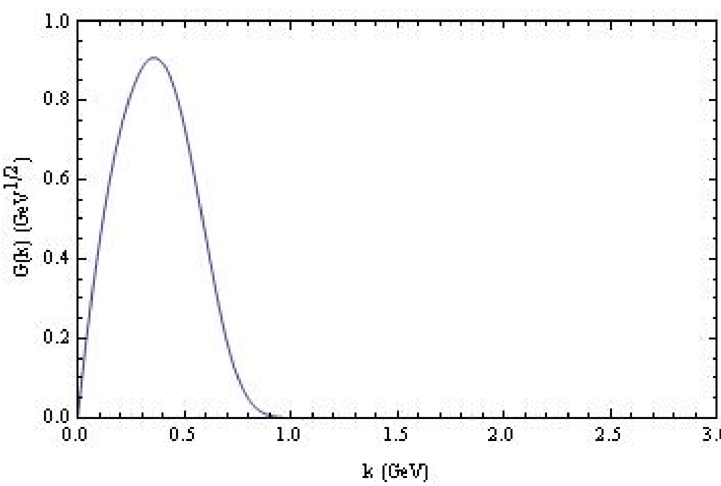

Fig. 4.3.1

By using the following parameter values from phenomenology[24][25]

$$f_{\rho\pi\pi} = 6.028$$

$$m_\rho = 0.770\ GeV$$

$$m_\pi = 0.138\ GeV$$

$$\Lambda = 0.585\ GeV$$

we find

$$m_{\rho 0} = 0.80404\ GeV$$

By (4.3.3), we can calculate the infinite volume phase shifts for ρ decay in the $\rho \to \pi\pi$ channel, as shown in Fig. 4.3.2.

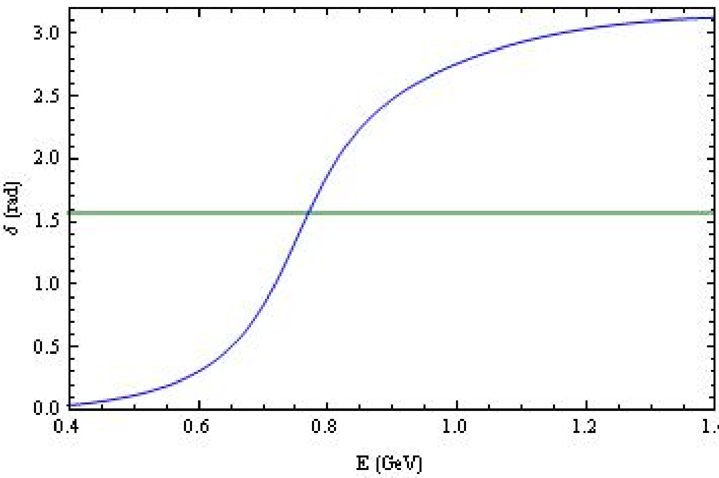

Fig. 4.3.2

4.4 Constructing the Hamiltonian

We will now construct a Hamiltonian and use it to get the energy spectrum for the $\rho \to \pi\pi$ scattering on the lattice, as we have done in Section 2.3. The Hamiltonian, in this case, is in the form

$$H = \begin{pmatrix} m_{\rho 0} & G_1 & G_1 & G_2 & G_2 & \cdots \\ G_1 & 2\omega_{k_1} & & & & \\ G_1 & & -2\omega_{k_1} & & & \\ G_2 & & & 2\omega_{k_2} & & \\ G_2 & & & & -2\omega_{k_2} & \\ \vdots & & & & & \ddots \end{pmatrix}$$

The energy eigenvalues of the Hamiltonian are

$$\lambda = m_{\rho 0} - 2\lambda \sum_n \frac{G_n^2}{E_n^2 - \lambda^2} \tag{4.4.1}$$

where

$$E_n = 2\omega_{k_n}$$

(4.4.1) matches the effective filed theory in the weak coupling limit where $|\lambda - E_n| \gg 0$. In this case $\lambda \simeq m_{\rho 0}$. So we can replace λ by $m_{\rho 0}$ in the right hand side and have

$$\lambda = m_{\rho 0} - 2m_{\rho 0} \sum_n \frac{G_n^2}{E_n^2 - m_{\rho 0}^2}$$

The ρ pole is identified by the solution of

$$E^2 = m_{\rho 0}^2 + \Sigma_{\rho\pi\pi}(E)$$

By expanding

$$\lambda^2 = m_{\rho 0}^2 + \Sigma_{\rho\pi\pi}(\lambda)$$

we have

$$\begin{aligned} \lambda &= \sqrt{m_{\rho 0}^2 + \Sigma_{\rho\pi\pi}(\lambda)} \\ &\simeq m_{\rho 0} + \tfrac{\Sigma_{\rho\pi\pi}(\lambda)}{2m_{\rho 0}} \end{aligned}$$

And in the weak coupling limit the ρ pole is identified by

$$m_\rho \simeq m_{\rho 0} + \frac{\Sigma_{\rho\pi\pi}(m_{\rho 0})}{2m_{\rho 0}}$$

So near the pole we have

$$m_\rho \simeq m_{\rho 0} - 2m_{\rho 0} \sum_n \frac{G_n^2}{(2\omega_{k_n})^2 - m_{\rho 0}^2} \tag{4.4.2}$$

and

$$m_\rho \simeq m_{\rho 0} + \frac{\Sigma_{\rho\pi\pi}(m_{\rho 0})}{2m_{\rho 0}} \tag{4.4.3}$$

We should choose G_n so that the two equations, (4.4.2) and (4.4.3), are the same. The discretized version of

$$\Sigma_{\rho\pi\pi}(E) = -\frac{f_{\rho\pi\pi}^2}{3\pi^3} \int d^3k' \frac{k'^2 u^2(k')}{(2\omega_{k'})((2\omega_{k'})^2 - E^2)}$$

is

$$\Sigma_{\rho\pi\pi}(E) = -\frac{f_{\rho\pi\pi}^2}{3\pi^3} (\frac{2\pi}{L})^3 \sum_n \frac{C_n k_n^2 u^2(k_n)}{(2\omega_{k_n})((2\omega_{k_n})^2 - E^2)}$$

So we have

$$\frac{\Sigma_{\rho\pi\pi}(m_{\rho 0})}{2m_{\rho 0}} = -\frac{1}{2m_{\rho 0}} \frac{f_{\rho\pi\pi}^2}{3\pi^3} (\frac{2\pi}{L})^3 \sum_n \frac{C_n k_n^2 u^2(k_n)}{(2\omega_{k_n})((2\omega_{k_n})^2 - m_{\rho 0}^2)}$$

and

$$\frac{\Sigma_{\rho\pi\pi}(m_{\rho 0})}{2m_{\rho 0}} = -2m_{\rho 0} \sum_n \frac{G_n^2}{(2\omega_{k_n})^2 - m_{\rho 0}^2}$$

Hence

$$G_n^2 = \frac{f_{\rho\pi\pi}^2}{24m_{\rho 0}^2\pi^3}(\frac{2\pi}{L})^3\frac{C_n k_n^2 u^2(k_n)}{\omega_{k_n}} \tag{4.4.4}$$

Here, L is the size of the lattice, C_n is the number of 3-D vectors $\overrightarrow{n} = (n_1, n_2, n_3)$ satisfying the condition $n_1, n_2, n_3 \in 0$ or $\mathbb{N}$ and the condition $|\overrightarrow{n}| = q \in \mathbb{N}$, and $k_n = \frac{2\pi}{L}q$. Then we can get the energy eigenvalues of the Hamiltonian by solving the equation

$$\lambda = m_{\rho 0} - 2m_{\rho 0}\frac{f_{\rho\pi\pi}^2}{24m_{\rho 0}\pi^3}(\frac{2\pi}{L})^3\sum_n \frac{C_n}{\sqrt{(\frac{2\pi q}{L})^2 + m_\pi^2}}\frac{k_n^2 u^2(k_n)}{4((\frac{2\pi q}{L})^2 + m_\pi^2) - \lambda^2}$$

for λ. In order not to have a Hamiltonian with too large a size, we take the form factor as

$$u(k_n) = \frac{e^{-\frac{k_n^4}{\Lambda^4}}}{e^{-\frac{p^4}{\Lambda^4}}}$$

and truncate the entries of the Hamiltonian at $u(k_n) \simeq 10^{-12}$.

4.5 Finding Finite Volume Phase Shifts

As in section 3.6, for the finite volume case, the allowed k's are

$$k = \frac{2\pi}{L}|\mathbf{n}|, \mathbf{n} \in \mathbb{Z}^3$$

From (2.7.1)

$$\phi(q) = \arctan(-\frac{\pi^{\frac{3}{2}}q}{\mathcal{Z}_{00}(1, q^2)})$$

where

$$\mathcal{Z}_{00}(1, q^2) = \frac{1}{\sqrt{4\pi}}(-\frac{1}{q^2} + J_0 + J_1 q^2 + \sum_{N=1}^{\infty} C_N \frac{q^4}{N^2(N - q^2)})$$

Hence we have

$$\delta = \arctan(\frac{\pi^{\frac{3}{2}}q}{\frac{1}{\sqrt{4\pi}}(-\frac{1}{q^2} + \sum_{m=1}^{\infty}(\frac{q^4}{m^2(m-q^2)} + \frac{q^2}{m^2}))})$$

Then, for the x-th lowest energy eigenvalue W_x, we have

$$\delta_x = \arctan(\frac{\pi^{\frac{3}{2}} q_x}{\frac{1}{\sqrt{4\pi}}(-\frac{1}{q_x^2} + \sum_{m=1}^{\infty}(\frac{q_x^4}{m^2(m-q_x^2)} + \frac{q_x^2}{m^2}))})$$

Since

$$W_x = 2\sqrt{k_x^2 + m_\pi^2}$$

we can replace q_x by $(\frac{L}{2\pi})\sqrt{\frac{W_x^2 - m_\pi^2}{4}}$ and have

$$\delta_x = \arctan(\frac{\pi^{\frac{3}{2}}(\frac{L}{2\pi})\sqrt{\frac{1}{4}W_x^2 - m_\pi^2}}{\frac{1}{\sqrt{4\pi}}(-\frac{1}{(\frac{L}{2\pi})^2(\frac{1}{4}W_x^2 - m_\pi^2)} + \sum_{m=1}^{\infty}(\frac{(\frac{L}{2\pi})^4(\frac{1}{4}W_x^2 - m_\pi^2)^2}{m^2(m-(\frac{L}{2\pi})^2(\frac{1}{4}W_x^2 - m_\pi^2))} + \frac{(\frac{L}{2\pi})^2(\frac{1}{4}W_x^2 - m_\pi^2)}{m^2}))}) \tag{4.5.1}$$

By (4.5.1), we can extract the phase shift of a specific energy eigenvalue through Lüscher's formalism.

As in Section 3.6, for numerical calculation, we make the upper limit for m adaptively increasable. In the codes, we compare the sum for $m = 1$ to n, denoted by S, and the sum for $m = n + 1$ to $n + 1000$, denoted by S_n. When $\frac{S_n}{S}$ is smaller than a certain acceptable value, then the loop is stopped, the upper limit is $m = n + 1000$, and $S + S_n$ is assigned to the sum. If not, then we increase m by 1000 and repeat the process. In this case we set $\frac{S_n}{S} < 5 \times 10^{-4}$.

We plot the phase shifts of the $\rho \to \pi\pi$ channel acquired by Lüscher's formula at different L's, as shown in Figs. 4.5.1 through 4.5.7.

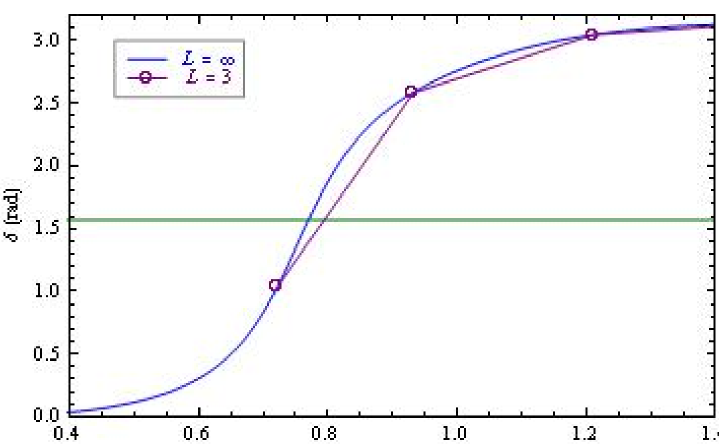

Fig. 4.5.1 Infinite volume phase shifts ($L = \infty$) and phase shifts at $L = 3$ (fm)

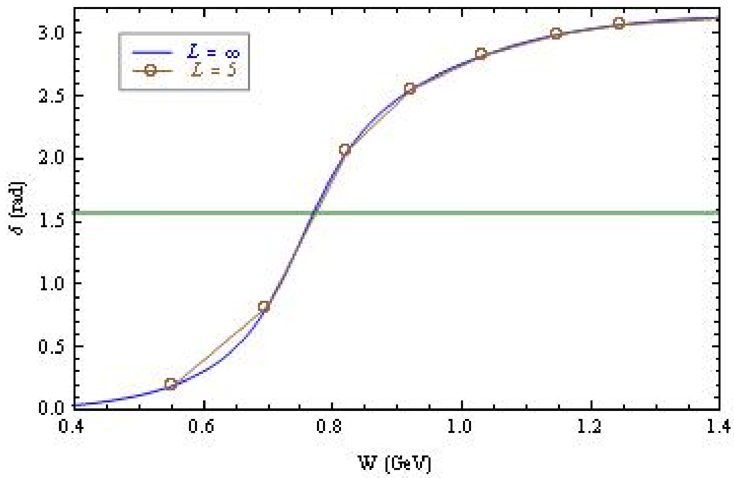

Fig. 4.5.2 Infinite volume phase shifts ($L = \infty$) and phase shifts at $L = 5$ (fm)

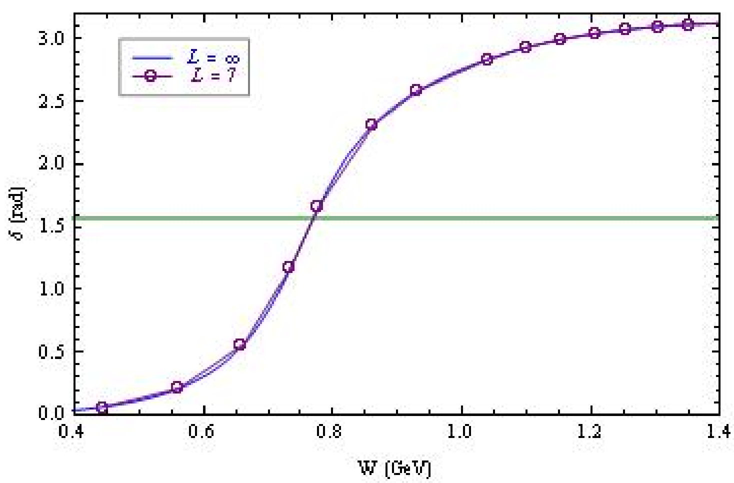

Fig. 4.5.3 Infinite volume phase shifts ($L = \infty$) and phase shifts at $L = 7$ (fm)

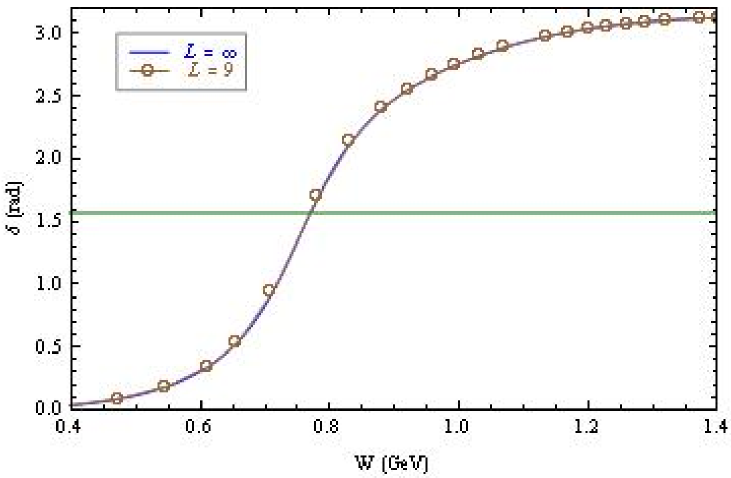

Fig. 4.5.4 Infinite volume phase shifts ($L = \infty$) and phase shifts at $L = 9$ (fm)

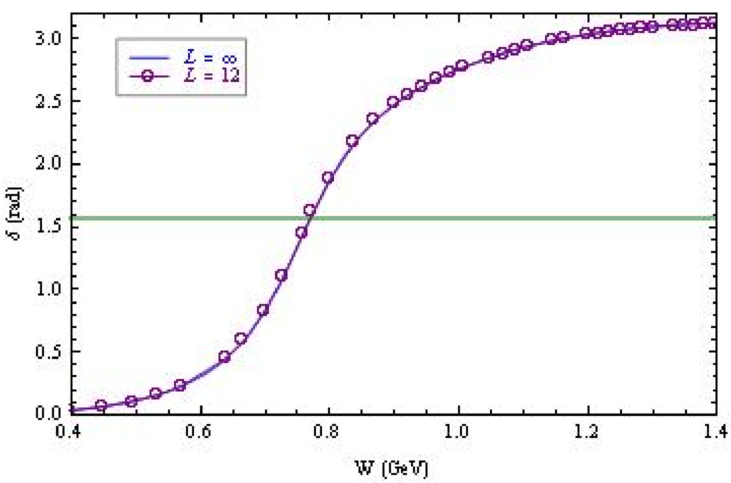

Fig. 4.5.5 Infinite volume phase shifts ($L = \infty$) and phase shifts at $L = 12$ (fm)

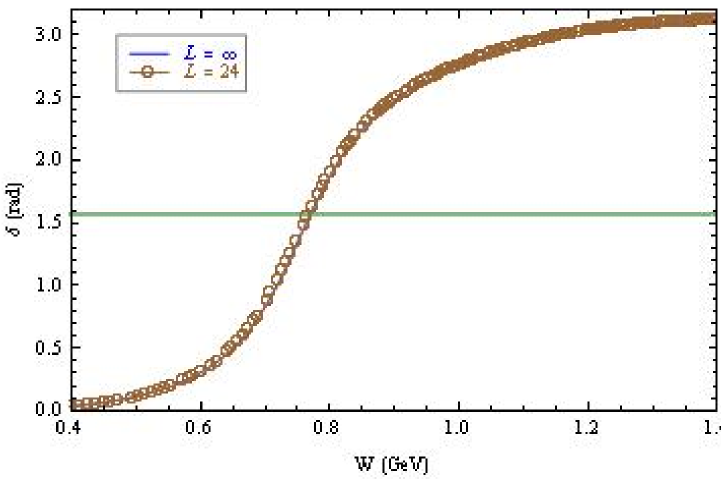

Fig. 4.5.6 Infinite volume phase shifts ($L = \infty$)
and phase shifts at $L = 24$ (fm)

To verify that finite volume phase shifts moves towards the infinite volume phase shifts as L increases, we find the finite volume phase shifts by interpolation at $W = 0.77$ (GeV) and $L = 3$ (fm), 5 (fm), 7 (fm), 9 (fm), 12 (fm), 24 (fm) as shown in Fig. 4.5.7.

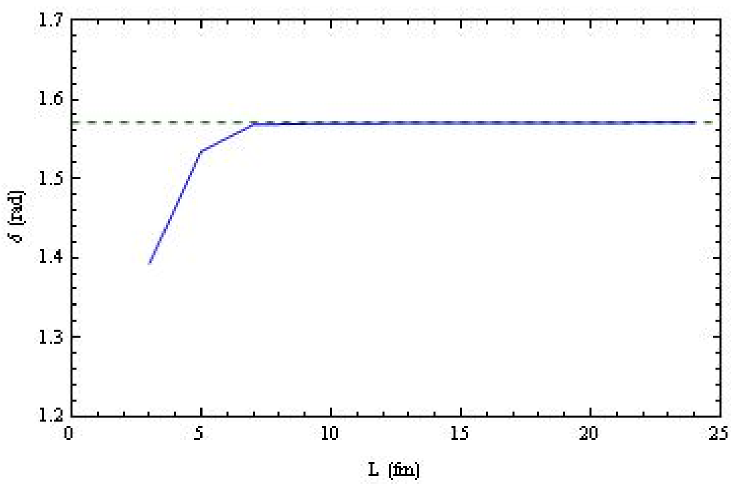

Fig. 4.5.7 Finite Volume Phase Shifts (Solid Lines) Compared
with Infinite Volume Phase Shifts (Dashed Lines)

In Fig. 4.5.7, we can observe that, as L increases, the finite volume phase shifts at all of the five different energies move towards the infinite volume phase shifts.

4.6 Inclusion of the Omega Meson

In this section we are going to include the ω meson. Hence, we include two coupled channels, that is, the $\rho \to \pi\pi$ channel in Fig. 4.1.1 and the $\rho \to \omega\pi$ channel in Fig. 4.1.2.

The self energy correction term arising from the $\rho \to \omega\pi$ channel is[23]

$$\Sigma_{\rho\pi\omega} = -\frac{f_{\rho\pi\omega}^2}{3\pi^2 f_\pi^2}\int dk' \frac{k'^4 u_{\pi\omega}^2(k')}{\sqrt{k'^2+m_\pi^2}(\sqrt{k'^2+m_\pi^2}+m_\omega - 2\sqrt{k^2+m_\pi^2})} \qquad (4.6.1)$$

where

$$f_{\rho\pi\omega} = \frac{g_{\rho\pi\omega} f_\pi}{2}\sqrt{m_\rho}$$

$$g_{\rho\pi\omega} = 16\ GeV^{-1}$$

$$f_\pi = 0.0924\ GeV$$

and the form factor is

$$u_{\pi\omega}(k') = e^{-\frac{k'^4}{\Lambda^4}}$$

To obtain the t-matrix in this case, we can replace $\Sigma_{\rho\pi\pi}$ in (4.3.1) by $\Sigma_{\rho\pi\pi} + \Sigma_{\rho\pi\omega}$ and get

$$\frac{G^2}{E - m_{\rho 0} - \frac{\Sigma_{\rho\pi\pi}(E^+)+\Sigma_{\rho\pi\omega}(E^+)}{2m_{\rho 0}}} = t(k,k,E^+) = -\frac{16 m_{\rho 0}}{\pi k} e^{-i\delta(k)} \sin\delta(k)$$

and the r-matrix is

$$\frac{G^2(k)}{E - m_{\rho 0} - \frac{P\Sigma_{\rho\pi\pi}(E)+P\Sigma_{\rho\pi\omega}(E)}{2m_{\rho 0}}} = r(k) = -\frac{16 m_{\rho 0}}{\pi k}\tan\delta(k)$$

By (4.6.1), as long as $k < \sqrt{\frac{m_\omega^2}{4} - m_\pi^2}$, there will be no pole in $\Sigma_{\rho\pi\omega}$.

We can get the value of $m_{\rho 0}$ by fitting it so that the pole occurs at m_ρ and r matrix goes to ∞. We use

$$G(k) = \sqrt{\frac{2f_{\rho\pi\pi}^2}{3\pi^2}}\frac{k u_{\pi\pi}(k)}{\sqrt{\omega_k}}$$

$$u_{\pi\pi}(k) = \frac{e^{-\frac{k^4}{\Lambda^4}}}{e^{-\frac{p^4}{\Lambda^4}}}$$

as in Section 4.3.

By using the following parameters from phenomenology[25]

$$f_{\rho\pi\pi} = 6.028$$

$$m_\rho = 0.770\ GeV$$

$$m_\omega = 0.782\ GeV$$

$$m_\pi = 0.138\ GeV$$

$$\Lambda = 0.585\ GeV$$

we find

$$m_{\rho 0} = 0.833\ GeV$$

The infinite volume phase shifts for ρ decay with $\rho \to \pi\pi$ and $\rho \to \pi\omega$ channels included are shown in Fig. 4.6.1.

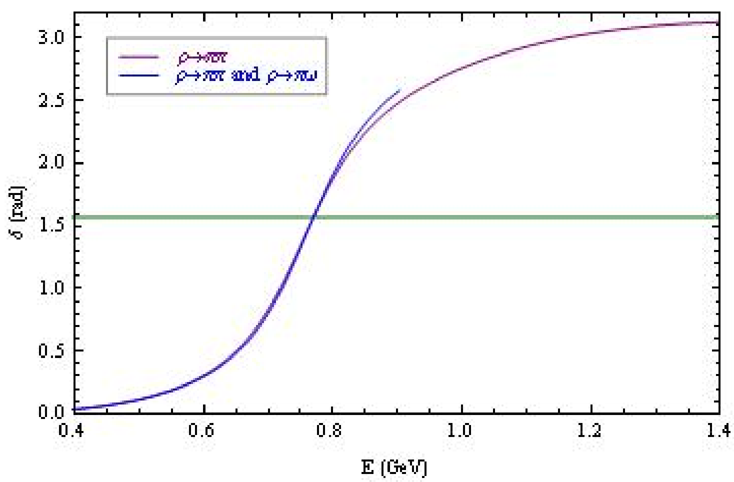

Fig. 4.6.1

4.7 Finite Volume Phase Shifts with Omega and Pion Included

The Hamiltonian incorporating the $\rho \to \pi\pi$ channel and the $\rho \to \pi\omega$ channel is

$$
H = \begin{pmatrix}
m_{\rho 0} & G_{\pi 1} & G_{\pi 1} & G_{\omega 1} & G_{\omega 1} & G_{\pi 2} & G_{\pi 2} & G_{\omega 2} & G_{\omega 2} & \cdots \\
G_{\pi 1} & 2\omega_{\pi 1} & & & & & & & & \\
G_{\pi 1} & & -2\omega_{\pi 1} & & & & & & & \\
G_{\omega 1} & & & \omega_{\pi 1} + \omega_{\omega 1} & & & & & & \\
G_{\omega 1} & & & & -(\omega_{\pi 1} + \omega_{\omega 1}) & & & & & \\
G_{\pi 2} & & & & & 2\omega_{\pi 2} & & & & \\
G_{\pi 2} & & & & & & -2\omega_{\pi 2} & & & \\
G_{\omega 2} & & & & & & & \omega_{\pi 2} + \omega_{\omega 2} & & \\
G_{\omega 2} & & & & & & & & -(\omega_{\pi 2} + \omega_{\omega 2}) & \\
\vdots & & & & & & & & & \ddots
\end{pmatrix} \tag{4.7.1}
$$

The energy eigenvalues are

$$
\lambda = m_{\rho 0} - 2m_{\rho 0} \sum_n \frac{G_{\pi n}^2}{E_{\pi n}^2 - \lambda^2} - 2m_{\rho 0} \sum_n \frac{G_{\omega n}^2}{E_{\omega n}^2 - \lambda^2} \tag{4.7.2}
$$

where

$$
\begin{aligned}
E_\pi &= 2\omega_\pi \\
&= 2\sqrt{k^2 + m_\pi^2}
\end{aligned}
$$

$$
\begin{aligned}
E_\omega &= \omega_\omega + \omega_\pi \\
&\simeq m_\omega + \sqrt{k^2 + m_\pi^2}
\end{aligned}
$$

The discretized version of (4.6.1)

$$
\Sigma_{\rho\pi\omega} = -\frac{f_{\rho\pi\omega}^2}{3\pi^2 f_\pi^2} \int dk' \frac{k'^4 u_{\pi\omega}^2(k')}{\sqrt{k'^2 + m_\pi^2}(\sqrt{k'^2 + m_\pi^2} + m_\omega - 2\sqrt{k^2 + m_\pi^2})}
$$

is

$$
\Sigma_{\rho\pi\omega} = -\frac{f_{\rho\pi\omega}^2}{3\pi^2 f_\pi^2} \left(\frac{2\pi}{L}\right)^3 \sum_n \frac{C_n k_n^2 u_{\pi\omega}^2(k_n)}{\omega_{\pi n}(E_{\omega n} - E)}
$$

So we have

$$\frac{\Sigma_{\rho\pi\omega}}{2m_{\rho 0}} = -\frac{1}{2m_{\rho 0}} \frac{f_{\rho\pi\omega}^2}{3\pi^2 f_\pi^2} \left(\frac{2\pi}{L}\right)^3 \sum_n \frac{C_n k_n^2 u_{\pi\omega}^2(k_n)(E_{\omega n}+E)}{\omega_{\pi n}(E_{\omega n}^2 - E^2)}$$

And we also have

$$\frac{\Sigma_{\rho\pi\omega}}{2m_{\rho 0}} = -2m_{\rho 0} \sum_n \frac{G_{\omega n}^2}{E_{\omega n}^2 - \lambda^2}$$

So we have $G_{\omega n}$ in (4.7.1) as

$$G_{\omega n} = \frac{f_{\rho\pi\omega}^2}{48 m_{\rho 0}^2 \pi^3 f_\pi^2} (\frac{2\pi}{L})^3 \frac{C_n k_n^2 u_{\pi\omega}^2(k_n)(E_{\omega n}+E)}{\omega_{\pi n}}$$

And we already have $G_{\pi n}$ as in (4.4.4)

$$G_{\pi n}^2 = \frac{f_{\rho\pi\pi}^2}{24 m_{\rho 0}^2 \pi^3} (\frac{2\pi}{L})^3 \frac{C_n k_n^2 u^2(k_n)}{\omega_{\pi n}}$$

With $G_{\omega n}$, $G_{\pi n}^2$, and (4.7.2), we can find the energy eigenvalues λ's.

Suppose one of the λ's has a value of W_x, then we can send it to (4.5.1) and get the finite volume phase shifts. In this case, we set $\frac{S_n}{S} < 5 \times 10^{-4}$ as in Section 4.5 and calculate the phase shifts at $L = 3$ (fm), 5 (fm), 7 (fm), 9 (fm), 12 (fm), and 24 (fm).

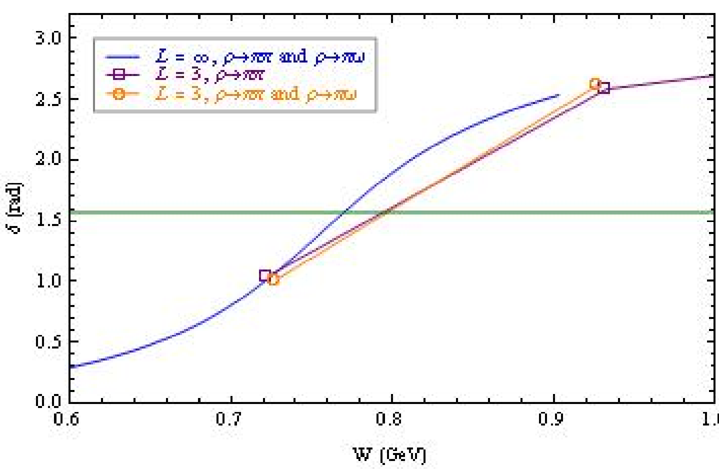

Fig. 4.7.1 Infinite volume phase shifts ($L = \infty$) and phase shifts at $L = 3$ (fm)

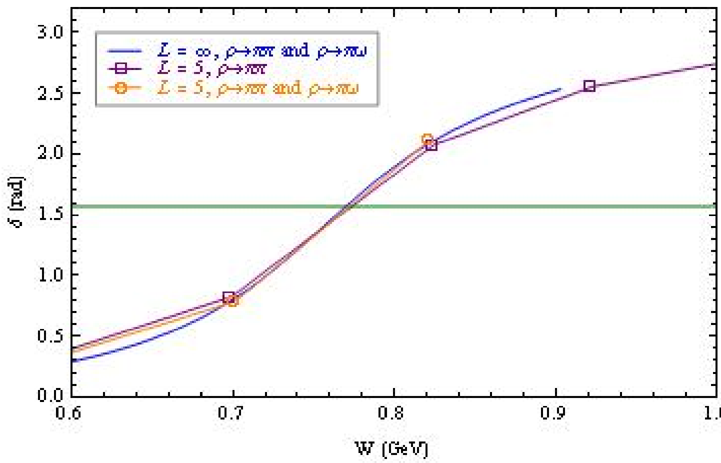

Fig. 4.7.2 Infinite volume phase shifts ($L = \infty$)
and phase shifts at $L = 5$ (fm)

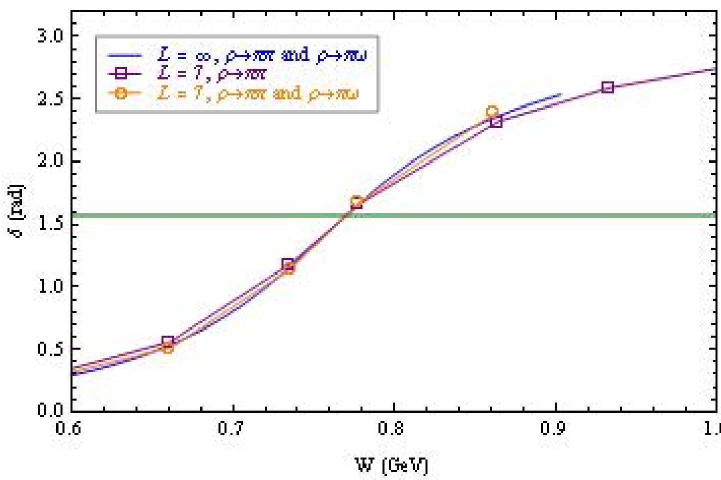

Fig. 4.7.3 Infinite volume phase shifts ($L = \infty$)
and phase shifts at $L = 17$ (fm)

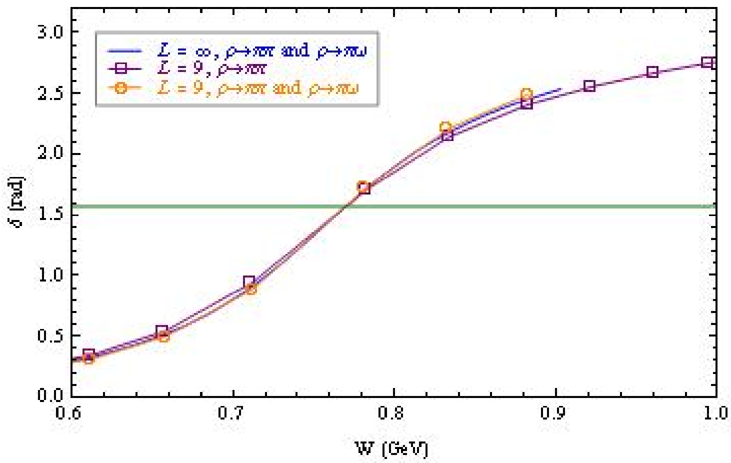

Fig. 4.7.4 Infinite volume phase shifts ($L = \infty$)
and phase shifts at $L = 19$ (fm)

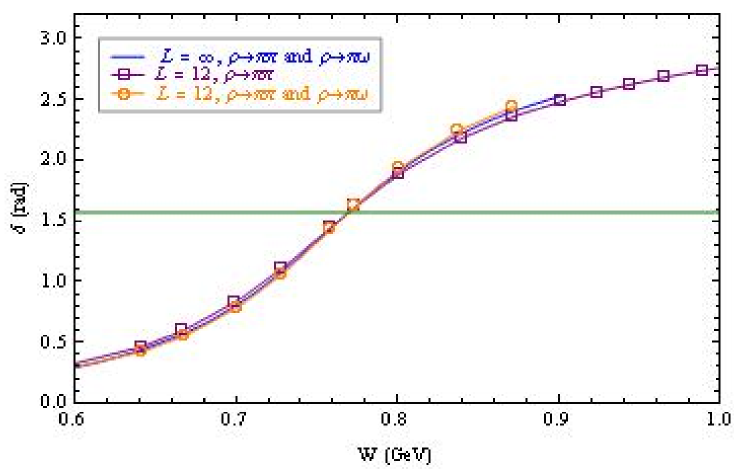

Fig. 4.7.5 Infinite volume phase shifts ($L = \infty$)
and phase shifts at $L = 12$ (fm)

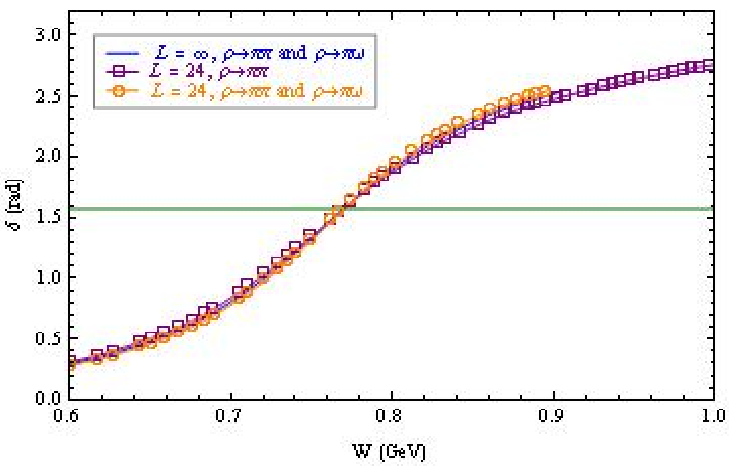

Fig. 4.7.6 Infinite volume phase shifts ($L = \infty$)
and phase shifts at $L = 24$ (fm)

To verify that finite volume phase shifts moves towards the infinite volume phase shifts as L increases, we find the finite volume phase shifts by interpolation at $W = 0.77$ (GeV) and $L = 3$ (fm), 5 (fm), 7 (fm), 9 (fm), 12 (fm), and 24 (fm).

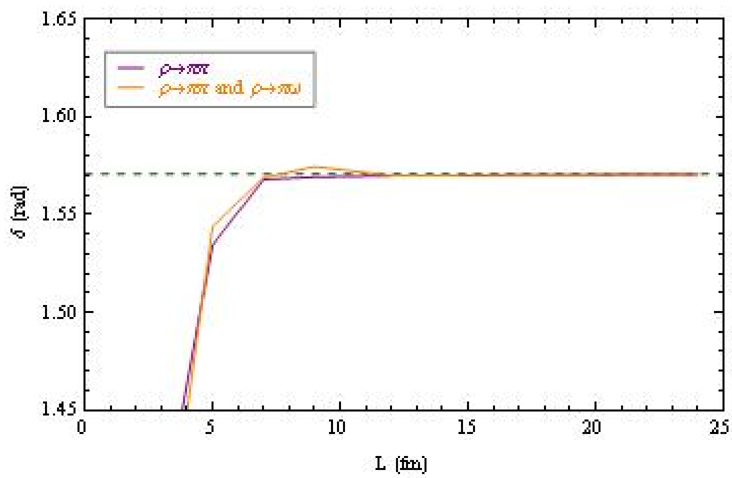

Fig. 4.7.7 Finite Volume Phase Shifts (Solid Line) Compared
with Infinite Volume Phase Shifts (Dashed Lines)

We also put the phase shifts where only $\rho \to \pi\pi$ channel is considered into Fig. 4.7.7 for comparison. We can observe that, as L increases, the finite volume phase shifts at $W = 0.77$ (GeV) moves towards the infinite volume phase shifts in both cases where only the $\rho \to \pi\pi$ channel is considered and where both $\rho \to \pi\pi$ and $\rho \to \pi\omega$ channels are included.

In Fig. 4.7.1 to Fig. 4.7.6, the finite volume phase shifts calculated from Lüscher's method are discrete dots and do not fall exactly on the pole position. We calculated the pole position by interpolation, which coresponds to the intersection of the straight line between the two closest dot below and above the pole and the horizontal line which marks $\delta = \frac{\pi}{2}$. In Fig. 4.7.1 to Fig. 4.7.6, all of the dots representing phase shifts extracted from Lüscher's formula lie very close to the curve of the exact infinite volume phase shift. This means that Lüscher's formula works quite well at $L > 3\ fm$. As discussed in Chapter 3, the problem of deciding the pole position comes from the scarce numbers of dots of phase shifts extracted from Lüscher's formula at small L values, which caused the deviations of the pole position calculated by interpolation.

As in Chapter 3, we calculate the difference ratio $\frac{\delta_L - \delta_\infty}{\delta_L}$. The difference ratio $\frac{\delta_L - \delta_\infty}{\delta_L}$ is plotted against L as shown in Fig. 4.7.8 for the case where only the $\rho \to \pi\pi$ channel is considered and in Fig. 4.7.9 for the case where both $\rho \to \pi\pi$ and $\rho \to \pi\omega$ channels are included.

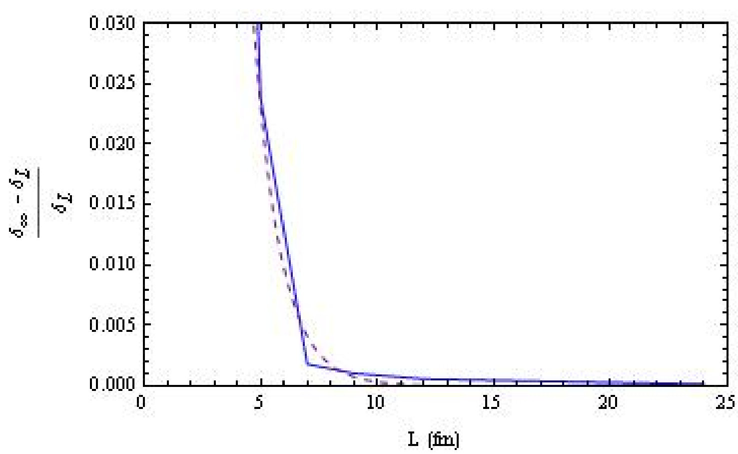

Fig. 4.7.8 Difference ratio between finite and infinite volume phase shifts (solid line) and its exponential fit (dashed line) of $\rho \to \pi\pi$ channel

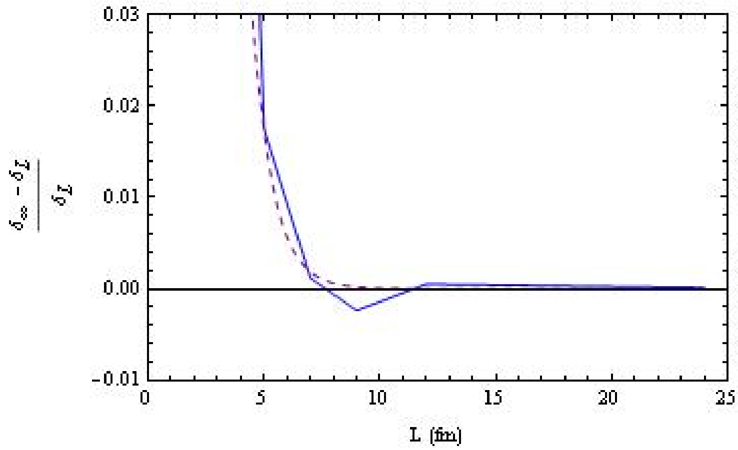

Fig. 4.7.9 Difference ratio between finite and infinite volume phase shifts (solid line) and its exponential fit (dashed line) of $\rho \to \pi\pi$ channel and $\rho \to \pi\omega$ channel

As in Chapter 3, we use an exponential fit to plot the relation between the difference ratio $\dfrac{\delta_L - \delta_\infty}{\delta_L}$ and L, which is shown as the dashed lines in Fig. 4.7.8 and Fig 4.7.9. In Fig. 4.7.8, the difference ratio in exponential fit diminishes as L increases. This result is in accordance with the decrease of finite volume effect at larger values of L as expected.

Chapter 5

Conclusion

5.1 Deviations of the Pole Position

In Chapter 3 we have calculated the infinite volume phase shifts and the finite volume phase shifts of $\sigma \to \pi\pi$ scattering. In Chapter 4 we have calculated the infinite volume phase shifts and the finite volume phase shifts of ρ decay in $\rho \to \pi\pi$ channel with and without the $\rho \to \pi\omega$ channel. We use a linear fit procedure to obtain the finite volume phase shifts at the pole position and denote it δ_L, where L is the side length of the lattice. At the pole position, the infinite volume phase shift, δ_∞, is $\frac{\pi}{2}$. We calculate the difference ratio $\frac{\delta_\infty - \delta_L}{\delta_L}$ for the $\sigma \to \pi\pi$ scattering and the ρ decay in the $\rho \to \pi\pi$ channel with and without the $\rho \to \pi\omega$ channel.

The dots which represent the finite volume phase shifts calculated by Lüscher's formula lie close to the curve of the exact infinite volume phase shift in all our calculations in Chapters 3 and 4. This shows that Lüscher's formula works quite well at the L values we have chosen. However, there are still deviations in pole positions in our calculations.

The deviation of the pole position calculated by Lüscher's formula can be attributed two factors. First, at small L values, the distribution of the energy eigenvalues of the Hamiltonian is scarce, and the pole position calculated by Lüscher's formula through interpolation is prone to be influenced by the positions of neighboring dots calculated by Lüscher's method from the energy eigenvalues. Second, although Lüscher's method works quite well, there is still the finite volume effect.

5.2 Lattice Effects

In the low energy region, QCD can not be studied perturbatively. Hence, lattice QCD is an important method for investigating QCD and the resonances in the lower energy region. However, the imposition of a lattice with periodic boundary conditions will cause discrepancies in the results of the finite volume models compared to the infinite volume results. Increasing the lattice size can reduce such discrepancies, but the cost is a huge demand in computational capacity.

Lüscher's formula can relate the energy spectra of finite volume models to infinite volume scattering processes. In this project, we have presented a finite volume model, extracted the energy eigenvalues, and found the corresponding phase shifts through Lüscher's formalism. We have applied our model to $\sigma \to \pi\pi$ scattering and ρ decay in the $\rho \to \pi\pi$ channel with and without the $\rho \to \pi\omega$ channel. For $\sigma \to \pi\pi$ scattering, the exponential fit of the difference ratio $\frac{\delta_\infty - \delta_L}{\delta_L}$ at the pole position is less than 1% when $L \gtrsim 21$ $(1/m_\pi)$. For ρ decay in the $\rho \to \pi\pi$ channel, the exponential fit of the difference ratio $\frac{\delta_\infty - \delta_L}{\delta_L}$ at the pole position is less than 0.01% when $L \gtrsim 12$ (fm). For the ρ decay in both the $\rho \to \pi\pi$ channel and the $\rho \to \pi\omega$ channel included, the exponential fit of the difference ratio $\frac{\delta_\infty - \delta_L}{\delta_L}$ at the pole position is at about 0.01% when $L \gtrsim 10$ (fm).

Because we extracted the finite volume phase shifts from the energy spectrum of the scattering system, the finite volume phase shifts are discretized. When there are not many energy eigenstates in the Hamiltonian, it is difficult to determine the pole position from the finite volume phase shifts. The problem is not so much the inaccuracy in Lüscher's method but the absence of a reliable way to get the pole position from calculated phase shifts when their distribution is sparse. We can find that, in order to keep the difference ratio $\frac{\delta_\infty - \delta_L}{\delta_L}$ small, we need the lattice side length larger than a certain value. This is understandable, since when L goes to ∞, the volume of the lattice becomes infinite, the model recovers the infinite volume scattering result, and the lattice effects decrease.

5.3 Prospect

We have presented the application of our model on the ρ meson. As a prospect, our model may also be used for investigating other resonances in the low energy region. For example, it can be used to investigate the excited states of the nucleons, such as the Δ baryon.[26]

For the Δ baryon, we can fit the Hamiltonian matrix with Λ, $g(0)$, and $m_{\Delta 0}$ as parameters to get the discrete energy spectra. With fitting technique and a good choice of regulator, the Hamiltonian matrix approach can improve the results calculated from Lüscher's method. An example of a good choice is a regulator in the dipole form.

The Hamiltonian matrix approach is also easier for calculation, since it can be difficult to generalize Lüscher's formula when we include more channels for the Δ baryon. If an additional channel is included, a new generalization of

Lüscher's formula might be needed. As for the Hamiltonian matrix, we only need to adjust its rows and columns adequately when more channels are included, and the Hamiltonian matrix approach can also help improve the results calculated from Lüscher's method when multiple channels are included. In addition to the Δ baryon, it can also be used to investigate other resonances.

Bibliography

[1] D. Griffiths. *Introduction to Elementary Particles.* USA: John Wiley & Sons (1987) 36 p.

[2] V. E. Barnes et al. Observation of a Hyperon with Strangeness -3 *Phys.Rev.Lett.,* 12:204-206, 1964.

[3] V. Bernard et al. Scalar mesons in a finite volume. *JHEP,* 1101:019, 2011.

[4] Photo courtesy Brookhaven National Laboratory.

[5] W. Weise. The QCD vacuum and its hadronic excitations. Lectures given at Conference: C04-08-22, St. Andrews, Scotland, Aug 22 - Aug 29, 2004. 201-232.

[6] C. Amsler et al. (Particle Data Group), PL **B667**, 1 (2008) (URL: http://pdg.lbl.gov).

[7] F. Gross. *Relativistic Quantum Mechanics and Field Theory.* John Wiley & Sons (1999) 581 p.

[8] H.-W. Lin and S. D. Cohen. Roper Properties on the Lattice: An Update. *AIP Conf. Proc.,* 1432:305-328, 2012.

[9] S. Dürr. A Proposal for topologically unquenched QCD. *Phys.Rev.,* D59:094501, 1999.

[10] D. B. Leinweber et al. Baryon masses from lattice QCD: Beyond the perturbative chiral regime. *Phys.Rev.,* D61:074502, 2000.

[11] D. Morel et al. Physical baryon resonance spectroscopy from lattice QCD. Contributed to Conference: C03-06-05, Durham, North Carolina, Jun 5 - Jun 10, 2003.

[12] G. Colangelo. Finite volume effects in chiral perturbation theory. *Nucl. Phys. Proc. Suppl.,* 140:120-126, 2005.

[13] G. Colangelo and S. Dürr. The Pion mass in finite volume. *Eur. Phys. J.,* C33:543-553, 2004.

[14] G. Colangelo and C. Haefeli. An Asymptotic formula for the pion decay constant in a large volume. *Phys. Lett.,* B590:258-264, 2004.

[15] G. Colangelo et al. Finite volume effects for meson masses and decay constants. *Nucl. Phys.,* B721:136-174, 2005.

[16] G. Colangelo et al. The pion and proton mass in finite volume. *Nucl. Phys. Proc. Suppl.* 153:41-48, 2006.

[17] M. Döring et al. Unitarized Chiral Perturbation Theory in a finite volume: Scalar meson sector. *Eur. Phys. J.,* A47:139, 2011.

[18] Y. Iwasaki. The CP - PACS project and lattice QCD results. *Prog. Theor. Phys. Suppl.,* 138:1-10, 2000.

[19] M. Döring and U. G. Meißner. Finite volume effects in pion-kaon scattering and reconstruction of the $\kappa(800)$ resonance. *JHEP,* 1201:009, 2012.

[20] M. Lüscher. Two-particle states on a torus and their relation to the scattering matrix. *Nucl. Phys.,* B354:531-578, 1991.

[21] M. Lüscher. Signatures of unstable particles in finite volume. *Nucl.* Phys., B364:237-254, 1994.

[22] G. B. Arfken and H. J. Weber. *Mathematical Methods for Physicists.* USA: Elsevier Academic Press (2005). 557 p.

[23] W. Armour et al. Unified chiral analysis of the vector meson spectrum from lattice QCD. *J. Phys.,* G32:971-992, 2006.

[24] D. B. Leinweber. Chiral behavior of the rho meson in lattice QCD. *Phys. Rev.,* D64:094502, 2001.

[25] J. Beringer et al. (Particle Data Group), PR **D86**, 010001 (2012) (URL: http://pdg.lbl.gov).

[26] J. M. M. Hall et al. A finite volume matrix Hamiltonian model for a $\Delta \to N\pi$ system. *Phys. Rev.,* D87:094510, 2013.